

## **UC Santa Cruz**

### **UC Santa Cruz Previously Published Works**

**Title**

Alternative source models of very low frequency events

**Permalink**

<https://escholarship.org/uc/item/5t24b5fb>

**Journal**

JOURNAL OF GEOPHYSICAL RESEARCH-SOLID EARTH, 121(9)

**ISSN**

2169-9313

**Authors**

Gomberg, J  
Agnew, DC  
Schwartz, SY

**Publication Date**

2016

**DOI**

10.1002/2016JB013001

Peer reviewed

## Alternative Source Models of Very Low Frequency Events

J. Gomberg<sup>1</sup>, D. C. Agnew<sup>2</sup>, and S.Y. Schwartz<sup>3</sup>

<sup>1</sup>U.S. Geological Survey, University of Washington, Seattle, Washington, USA

<sup>2</sup>Institute of Geophysics and Planetary Physics, University of California San Diego, La Jolla, California, USA

<sup>3</sup>Department of Earth and Planetary Sciences, University of California Santa Cruz, Santa Cruz, California, USA

### Key Points:

- Clustered arrivals of  $M_w < 2$  Low Frequency Earthquake signals (LFEs) can explain characteristics of Very Low Frequency (VLF) events.
- Temporally clustered LFE sources may be triggered by a single larger, or many smaller distinct aseismic slip events, or occur by chance.
- VLF events may not bridge the gap between  $M_w > \sim 5$  slow slip transients and LFEs.

## 18 **Abstract**

19 We present alternative source models for very low frequency (VLF) events, previously  
20 inferred to be radiation from individual slow earthquakes that partly fill the period range  
21 between slow slip events lasting thousands of seconds and low frequency earthquakes  
22 (LFE) with durations of tenths of a second. We show that VLF events may emerge from  
23 band-pass filtering a sum of clustered, shorter duration, LFE signals, believed to be the  
24 components of tectonic tremor. Most published studies show VLF events occurring  
25 concurrently with tremor bursts and LFE signals. Our analysis of continuous data from  
26 Costa Rica detected VLF events only when tremor was also occurring, which was only  
27 seven percent of the total time examined. Using analytic and synthetic models, we show  
28 that a cluster of LFE signals produces the distinguishing characteristics of VLF events,  
29 which may be determined by the cluster envelope. The envelope may be diagnostic of a  
30 single, dynamic, slowly slipping event that propagates coherently over kilometers, or  
31 represent a narrowly band-passed version of nearly simultaneous arrivals of radiation  
32 from slip on multiple higher stress drop and/or faster propagating slip patches with  
33 dimensions of tens of meters (i.e., LFE sources). Temporally clustered LFE sources may  
34 be triggered by single or multiple distinct aseismic slip events, or represent the nearly  
35 simultaneous chance occurrence of background LFEs. Given the non-uniqueness in  
36 possible source durations, we suggest it is premature to draw conclusions about VLF  
37 event sources or how they scale.

38

## 39 **1. Introduction**

40 ‘Very low frequency’ events refer to pulses of energy observed in seismic data in the .02-  
41 .05 Hz frequency band. These have been thought to represent seismic waves radiated  
42 from fault slip events with magnitude  $M_w$  2-5 with lower stress drops and slower rupture  
43 velocities than ordinary earthquakes. Hereafter we use the common nomenclature VLF  
44 events to refer to these transient signals, while proposing alternative interpretations of  
45 what processes they may result from. Numerous authors have suggested that the sources  
46 of VLF events bridge the period gap between transient slow slip events with large  
47 moments ( $M_0 > \sim 10^{17}$  N-m or moment magnitude  $M_w > \sim 5.5$ ) and durations of days to years,  
48 and low frequency earthquakes, with very small moments ( $M_0 < \sim 10^{12}$  N-m or  $M_w < \sim 2.0$ )

49 and durations of fractions of a second. The former radiate negligible seismic energy and  
50 typically are measured geodetically, while the latter are inferred to rupture slowly relative  
51 to ordinary earthquakes of the same moments but still fast enough to radiate measurable  
52 seismic signals [*Ide et al.*, 2007a; 2007b; 2008; *Ito et al.*, 2009; *Matsuzawa et al.*, 2009a;  
53 *Takeo et al.*, 2010; *Ide and Yabe*, 2014]. These small events are called low frequency  
54 earthquakes (LFE) because they are depleted in high frequency energy relative to typical  
55 earthquakes with comparable low frequency spectral amplitudes.

56

57 Here we introduce a few features of LFE signals relevant to this study, with more  
58 discussion provided in Section 2. LFE occurrence and transient slow slip appear to be  
59 causally linked based on correlations between their rates and estimated source locations,  
60 and both are inferred to represent release of tectonic stresses via shear slip along plate  
61 interfaces, with the slow slip being the primary mode of release [*Ide et al.*, 2007a; *Frank*  
62 *et al.*, 2013; *Royer and Bostock*, 2014]. LFE signals also appear to cluster spatially and  
63 temporally [*Shelly et al.*, 2007; *Frank et al.*, 2014; *Sweet et al.*, 2014; *Bostock et al.*,  
64 2015; *Savard and Bostock*, 2015; *Frank et al.*, 2016], and are thought to be the building  
65 blocks of tremor, a term which describes emergent, quasi-continuous, low-amplitude,  
66 seismic signals that correlate over distances of tens of km or more [*Shelly et al.*, 2006].

67

68 We present an alternative model for the origin of VLF events. We suggest that, instead  
69 of representing the seismic radiation from  $M_w$  2-5 slow earthquakes, some VLF events  
70 may be simply the result of narrowband filtering of clustered arrivals of much smaller  
71 signals from  $M_w < 2$  LFEs. In a single slip event, the physics of dynamic rupture governs a  
72 process of coherent slip propagation, and the temporal and spatial scales of this process  
73 determine the characteristics of the radiated seismic energy. The complete spectrum of  
74 waves radiated from an event propagating coherently over tens of km and hundreds of  
75 seconds will differ from the spectrum of a sum of smaller slip events, each propagating  
76 only tens of meters within fractions of a second. But as we show, this difference may not  
77 be distinguishable using only observations in narrow frequency bands. To highlight the  
78 non-uniqueness in interpretation of such observations, we note here that while linking  
79 VLF events with tremor bursts is common to both the models we propose and the one

80 presented in *Ide* [2008], the models differ in fundamental ways; in particular, *Ide*'s model  
81 [*Ide*, 2008] suggests that VLF events represent radiation directly resulting from larger  
82 slow slippage and that LFE signals may be artifacts of limited detection capabilities (see  
83 Section 6 for more discussion).

84

85

86 We illustrate the difference between sources of a single, larger slip event and a sum of  
87 smaller ones by considering the more familiar and analogous cases of aftershocks and  
88 afterslip, and earthquake swarms and accompanying slow, aseismic slip. Repeating  
89 earthquakes also are now often used to infer characteristics of driving slow, aseismic slip  
90 [*Nadeau and McEvilly*, 1999; *Gardonio et al.*, 2015; *Lengliné and Ampuero*, 2015]. In  
91 general, the moment of the aseismic slip substantially exceeds that of cumulative moment  
92 of the seismic events and thus, the former likely drives the latter [*Peng and Gombert*,  
93 2010]. Often only the seismic signals are observable, and while they provide clues that  
94 aseismic slip is underway, one would not use the envelope of the aftershocks, repeaters,  
95 or swarm earthquakes to infer details or even gross features (e.g., the total moment) of the  
96 afterslip or driving slow slip.

97

98 If LFEs are a response to transient slow slip, similar caution should be employed when  
99 using their aggregate signals to infer the characteristics of whatever drives them,  
100 particularly when only a narrow frequency band of the aggregate signal is examined.  
101 Simulation of moderate to large earthquakes also illustrates the important distinction  
102 between a single larger slip event and a cascade or sum of smaller ones. Nearly all  
103 methods to simulate earthquakes as distributed sources invoke a discretized form of the  
104 representation theorem, which describes the displacement field at some distance from the  
105 fault as an integral over the fault plane of the product of the slip history and a Green's  
106 function describing the medium response [*Aki and Richards*, 1980]. Small earthquake  
107 seismograms may be used as Green's functions distributed over points on the rupture  
108 plane, weighted and filtered by a model of the slip history (source model) at each  
109 corresponding point (see *Hartzell et al.*, [1999] for a summary). A source model  
110 representing the coherent propagation of slip determines the weightings and phase shifts  
111 used to sum the Green's functions, and is required to reproduce the complete spectrum

112 correctly [*Frankel, 1995; Hartzell et al., 1999*]. Summing independent, randomly  
113 distributed LFE signals is equivalent to using random weightings and phase shifts;  
114 effectively, using no source model. It would then make no sense to measure the summed  
115 signals and infer a source model, as one does not exist.

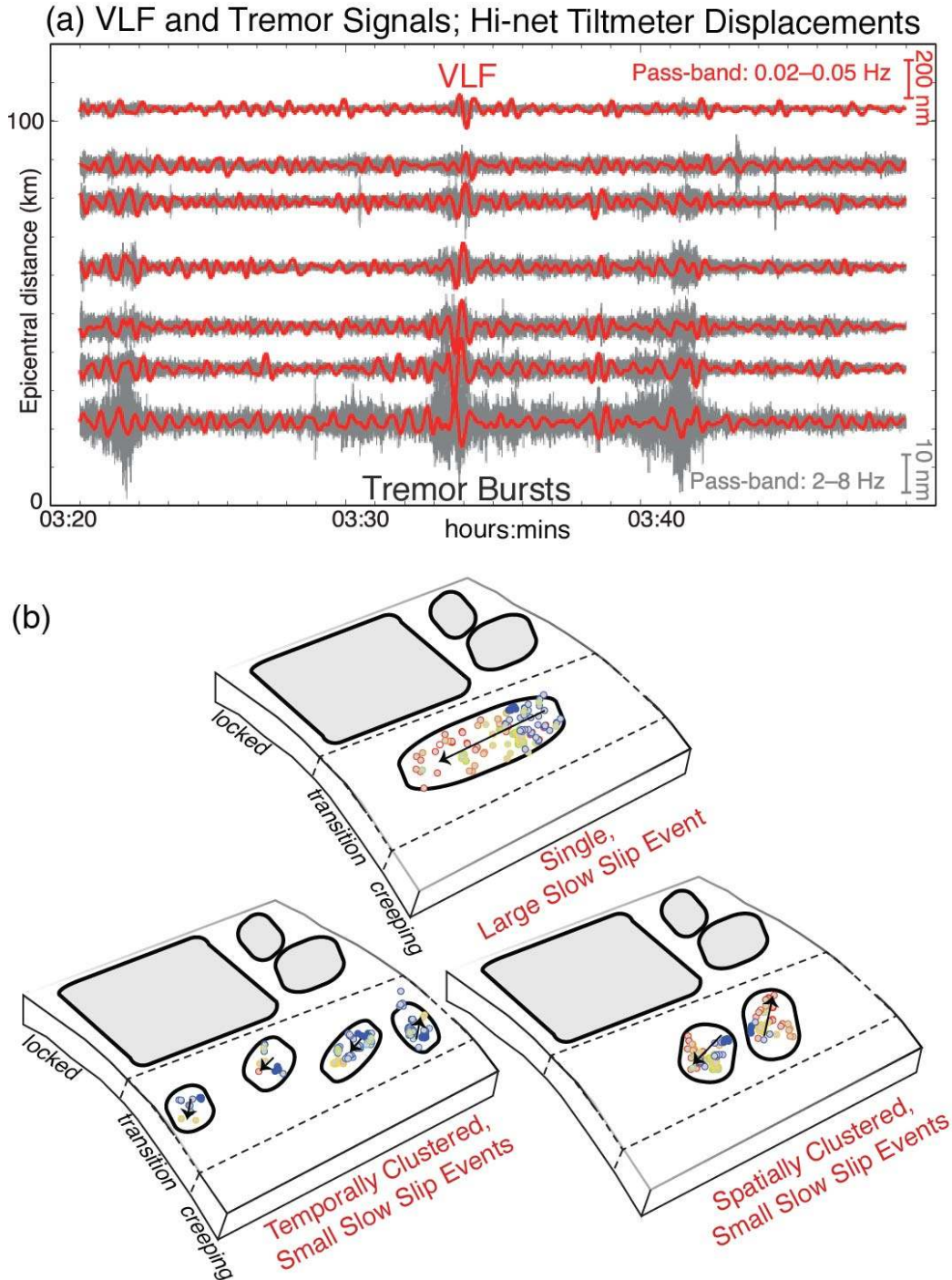
116

117 In Section 2 we describe the characteristics of VLF and LFE observations, and of tremor  
118 that any interpretations should explain or be consistent with. We then present an analytic  
119 model of a clustered series of LFE signals (Section 3), simulations using synthetic signals  
120 (Section 4), and a test using observations of tremor and VLF events from Costa Rica  
121 (Section 5).

122

## 123 **2. VLF, LFE and tremor characteristics**

124 VLF events refer to pulses of seismic energy with durations of tens to several hundred  
125 seconds, inferred to represent waves radiated from fault slip events with  $M_w \sim 2-5$  (Fig. 1,  
126 modified from *Ito et al. [2007]*), which contrast with LFE signals that originate from  
127 smaller slow earthquakes ( $M_w \sim 1$  to 1.5), which last less than a few seconds, and radiate  
128 most often in the 2-8 Hz passband (see the Introduction in *Sweet et al. [2014]* for more  
129 background). Characteristics attributed to the inferred source of VLF events include  
130 significantly lower stress drops and/or slower rupture velocities than ordinary  
131 earthquakes. Tremor also belongs to the class of slow earthquakes, and a number of  
132 studies have suggested that tremor may be comprised of a superposition of LFE signals  
133 [*Shelly et al., 2006; 2007; Ide et al., 2008; Chamberlain et al., 2014; Frank et al., 2014*].  
134 In some studies the spectra of these slow seismic signals appear to decay as  $\sim f^{-1}$  rather  
135 than  $\sim f^{-2}$  measured for many fast earthquakes [*Ide et al., 2007b; Rubinstein et al., 2010*],  
136 and in others both tremor and fast earthquakes decay as  $\sim f^{-2}$  [*Fletcher and McGarr,*  
137 *2011; Zhang et al., 2011*]. In various ways these studies attempted to account for the  
138 spectral decay due to attenuation. [*Gomberg et al., 2012*] showed that in some instances  
139 spectral decay rate differences between earthquakes and LFEs may be attributed to near-  
140 source attenuation rather than source differences.



141

142 **Figure 1.** Examples of VLF waveforms and inferred source models. (a) Displacement  
 143 waveforms derived from radial-component tiltmeter signals recorded by the Japanese Hi-  
 144 net network at a range of source-receiver distances, after band-pass filtering in the .02-.05  
 145 Hz (red) and 2-8 Hz (grey) pass-bands to illuminate VLF events and tremor, respectively.  
 146 Modified from *Ito et al.*'s [2007] Figure 1. (b) Cartoons of fault surfaces, with features of  
 147 *Ito et al.*'s [2007] Figure 4, with three different LFE source models that might give rise to  
 148 indistinguishable clustered LFE arrivals, tremor bursts and VLF events. A velocity-

149 strengthening background contains velocity-weakening patches. In the shallower ‘locked’  
150 zone, large patches (grey polygons) slip in earthquakes. In the transition zone slip occurs  
151 in transient, mostly aseismic slow slip episodes within outlined polygons that contain tiny  
152 patches (circles with colors and arrows indicating relative failure times). See text.  
153

154 Another noteworthy characteristic of VLF events is that in almost all cases they are  
155 observed with concurrent tremor, particularly during bursts of tremor activity [*Ito and*  
156 *Obara*, 2006a; *Ito et al.*, 2007; *Ide et al.*, 2007a; 2007b; 2008; *Ito et al.*, 2009; *Matsuzawa*  
157 *et al.*, 2009a; *Takeo et al.*, 2010; *Walter et al.*, 2013; *Frank et al.*, 2014; *Ide and Yabe*,  
158 2014; *Ghosh et al.*, 2015; *Savard and Bostock*, 2015; *Yamashita et al.*, 2015; *Ide*, 2016].  
159 *Ide et al.* [2008] identified and measured VLF events by fitting theoretical moment-rate  
160 functions to seismic displacement data band-pass filtered between .005-.05 Hz during  
161 time intervals with clear tremor, and noted that the moment-rate functions estimated have  
162 nearly identical shapes to the envelopes of the squared seismic velocities in the tremor  
163 band-pass of 2-8 Hz. Notably, they inferred that VLF event sources and LFEs most likely  
164 are each triggered by concurrent surrounding, slower, and larger slip, but they also noted  
165 that the VLF events could be a superposition of those from LFEs. *Ide and Yabe* [2014]  
166 used the timing of tremor bursts to stack broadband seismograms in order to detect VLF  
167 events in western Japan. Their stacking procedure revealed that high frequency tremors  
168 are accompanied by VLF events in all regions with tremor in western Japan and that the  
169 seismic energy of the tremor and the seismic moment in the VLF band are proportional.  
170 They argued that the ubiquity of VLF events provides support for the idea of a continuum  
171 of slow slip phenomena from the tremor band through the geodetic observations of slow  
172 slip. Finally, [*Ide*, 2008] proposed a model linking VLF events to LFEs and tremor,  
173 which we discuss more thoroughly in Section 5.

174

175 The studies of *Ito et al.* [2007, 2009], *Matsuzawa et al.* [2009], *Takeo et al.* [2010] also  
176 suggest that LFEs and sources of VLF events are members of a continuum of slow slip  
177 events. The two studies of *Ando et al.* [2012], *Asano et al.* [2008] and [*Hutchison and*  
178 *Ghosh* [2016] identified VLF events but not tremor. However, in the Asano and Ando  
179 studies the occurrence of tremor accompanying their VLF observations from Japan  
180 cannot be ruled out, at least based on information provided, because neither publication



181 mentions a search for tremor [Asano *et al.*, 2008; Ando *et al.*, 2012]; their analyses  
182 focused on data filtered in the VLF pass-band of .02-.05 Hz and only examined data at  
183 frequencies in the tremor pass-band (> 1 Hz) to search for potentially contaminating  
184 earthquakes, without specifying how the search was conducted [Ando *et al.* 2012] or  
185 searching only in time windows when earthquakes were cataloged [Asano *et al.* 2008].  
186 Moreover, the results reported in Ando *et al.* [2012] may indicate that the VLF events  
187 were sums of LFEs that originated from multiple locations and arrived in clusters, as they  
188 noted 'complicated waveforms' for over 50% of the 1314 VLF events identified and of  
189 the 120 with locations and focal mechanisms estimated, only 18% were considered robust  
190 and 27% had complex waveforms and scattered locations. Hutchison and Ghosh [2016]  
191 found eight VLF events during an ~90 day interval during the 2014 Cascadia 'episodic  
192 tremor and slip' event, which located in a region lacking 'strong' tremor activity. The low  
193 signal to noise and monochromatic nature of the data, coupled with poor fits between  
194 data and synthetic waveforms (variance reduction of 47%) for the single example of a  
195 centroid moment tensor inversion of a VLF event shown, casts some doubt on these  
196 findings- Notably perhaps, Hutchison and Ghosh [2016] conclude that "while we cannot  
197 entirely rule out that some of the initial detections are in fact real, we only include events  
198 with robust moment tensor solutions".

199  
200 If tremor is comprised of LFE signals (see next paragraph, and Shelly *et al.* [2006]), then  
201 arrivals of spatially and/or temporally clustered LFE signals would manifest as tremor  
202 bursts and possibly VLF events. Indeed, while detection methods that rely on correlation  
203 and waveform similarity will pick out LFEs with spatially clustered sources [Bostock *et*  
204 *al.*, 2012; Frank *et al.*, 2014; Royer and Bostock, 2014; Bostock *et al.*, 2015; Frank *et al.*,  
205 2016], they also commonly cluster temporally as well [Shelly *et al.*, 2007; Frank *et al.*,  
206 2014; Sweet *et al.*, 2014; Bostock *et al.*, 2015; Savard and Bostock, 2015; Frank *et al.*,  
207 2016]. Sweet *et al.* [2014] studied recurring clusters, or 'families', in Cascadia and  
208 found a single family would be active for 10 minutes to 12 hours. In their analysis of LFE  
209 families in Mexico, Frank *et al.* [2014] found LFE families activated in bursts, with inter-  
210 event recurrence intervals of <10 seconds.

211

212 We propose that in some cases, VLF events result from temporally clustered arrivals of  
213 LFE signals, suggested by the fact that VLF events almost always are simultaneous with  
214 tremor bursts. This proposition thus relies on the assumption that tremor is a  
215 superposition of LFE signals, as first proposed in [Shelly *et al.*, 2006]. We justify this  
216 assumption with a brief review of the evidence for it. To our knowledge, in most studies  
217 LFEs detected within tremor comprise only a fraction of the tremor, but we suggest that it  
218 is impossible to know whether this reflects physical processes or detection biases. For  
219 example, in their study of LFEs in Guerrero Mexico, Frank *et al.* [2014] found only 35%  
220 of the tremor contained LFEs. LFEs appear to be more abundant in the northern portions  
221 of Cascadia, but nowhere account for all the tremor [Bostock *et al.*, 2015; Savard and  
222 Bostock, 2015]. Nearly all LFE detection methods impose restrictive detection criteria,  
223 thus implicitly selecting only a subset of LFEs and resulting in an incomplete LFE  
224 catalog. These methods rely on waveform similarity, either at multiple recording stations  
225 in a network (e.g., beam-forming methods) and/or between LFEs at multiple times (e.g.,  
226 match-filtering and stacking methods). The requirement for cross-station similarity  
227 means detections are possible only when propagation and site effects are similar at  
228 network stations, proposed as an explanation for the geographic variation in LFE rates in  
229 Cascadia [Rubin and Armbruster, 2013; Armbruster *et al.*, 2014; Savard and Bostock,  
230 2015]. Methods reliant on waveform similarity between multiple LFEs will detect only  
231 sources that recur with nearly the same location and mechanism. The results of Frank *et*  
232 *al.* [2014] suggest that this may eliminate many LFEs that do not repeat, noting that their  
233 application of a beam-forming method yielded many thousands of LFE detections but an  
234 “enormous amount of events” did not meet the coherence requirements of their second-  
235 step stacking procedure. In addition to detection biases, real physical processes may  
236 hamper the ability to unravel individual LFEs from tremor, and lead to real variations in  
237 how LFEs cluster temporally and spatially. The source dimensions of LFEs, and how  
238 they scale and recur, likely depends on differential stresses and frictional properties,  
239 properties that surely vary temporally and spatially [Wech and Creager, 2011; Bostock *et*  
240 *al.*, 2015]. Additionally the amplitudes radiated by LFEs may reflect variations in the  
241 slow slip inferred to drive them, which surely also varies temporally and spatially  
242 [Bostock *et al.*, 2015].

243

244 Finally we consider how clustering may arise, noting that many ways appear plausible,  
245 making it difficult to infer uniquely what slow slip may drive it [*Sweet et al.*, 2014;  
246 *Bostock et al.*, 2015; *Frank et al.*, 2016]. Figure 1b illustrates just a few of the models of  
247 LFE sources and driving slow slip that might radiate signals that arrive in similarly  
248 clustered bursts. These models are based on ideas of *Ide* [2014] and other studies  
249 referenced therein, in which the properties of the fault surface may be described by  
250 elastic, velocity-weakening patches (gray areas within polygons or gray and blue shaded  
251 tiny circles) within a viscous, velocity-strengthening background, and in which fracture  
252 energy increases with patch size [*Ide*, 2014]. In the shallower ‘locked’ zone, large  
253 patches cover most of the surface so tectonic stress relaxation occurs primarily through  
254 fast, dynamic slip with relatively large stress drops (i.e. earthquakes). In the ‘transition’  
255 zone, the properties of the background dominate and transient, slow, essentially aseismic  
256 slip with low stress drops relaxes tectonic stressing. Low amplitude LFE signals radiate  
257 from the tiny patches whose failure is triggered by the passing slow slip front, either  
258 immediately or with some delay. LFEs may radiate waves that arrive in clustered bursts,  
259 but originating from a variety of different temporal and spatial source distributions  
260 (illustrated schematically in Fig. 1b). The driving process underlying each of these  
261 distributions may differ quite significantly.

262

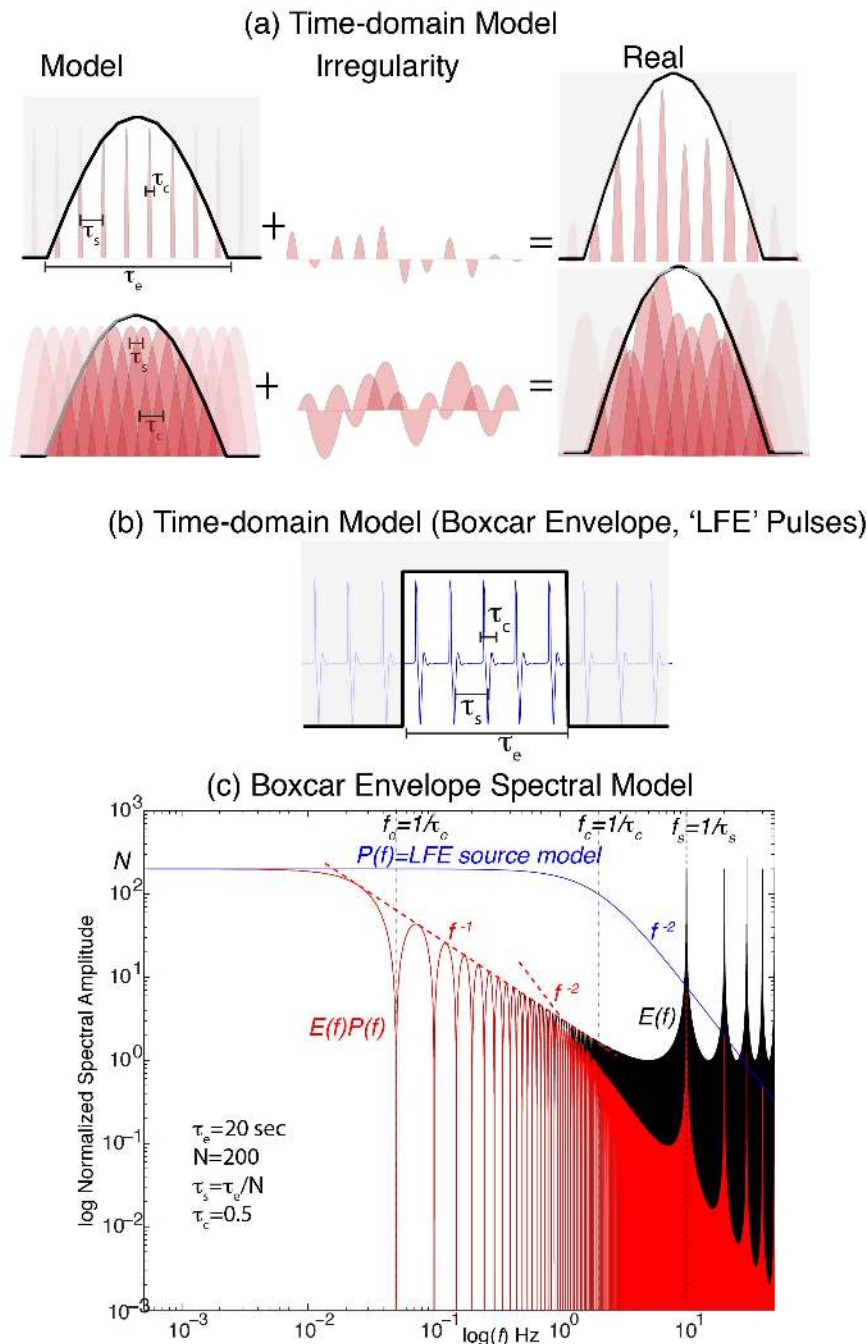
263 The study of *Frank et al.* [2016] suggests an important, but indirect role of slow slip in  
264 the evolution of LFE activity. They study LFE activity in Mexico and conclude that  
265 transient slow slip may promote the conditions required for interactions and clustering,  
266 but a variety of interaction mechanisms may be in play (e.g., dynamic or static stress  
267 transfer). They showed LFEs to be highly clustered spatially and temporally, and  
268 interpreted aspects of the clustering as evidence for interactions between LFE sources  
269 (measured using a variety of metrics). Importantly, slow slip was accompanied not just  
270 by an increase in the rate of LFEs but the degree to which they clustered and interacted  
271 with one another, which they showed related to an increased spatial density of critically  
272 stressed LFE source patches promoted by surrounding slow slip. In addition, clustered  
273 LFEs likely occur in the absence of larger-scale slow slip transients, either because their

274 sources interact as inferred in *Frank et al.* [2016], or by chance as a Poisson process  
275 similar to ‘background’ seismicity [*Michael*, 2012].

276

### 277 **3. Analytic Clustered LFE Model**

278 In this Section, we consider a mathematical model of VLF events represented as a  
279 clustered arrival of signals from rapid slip events, evident as a finite series of pulses or  
280 LFEs. Figure 2a shows the model proposed (labeled “Model”) where a series of LFEs  
281 each with time constant  $\tau_c$  (subscript ‘c’ consistent with other publications in which  $\tau_c$   
282 approximates the inverse of the source ‘corner’ frequency,  $f_c$ ) are separated by a time  $\tau_s$ ,  
283 and the whole sequence has an overall envelope with time constant  $\tau_e$ . This idealized  
284 sequence (labeled “Model” in Fig. 2a) is only an approximation to real sequences of  
285 LFEs (labeled “Real” in Fig. 2a), which may be envisioned by adding the middle series to  
286 the idealized one. We propose that the idealized model predictions capture the key  
287 features of a cluster of LFE signal arrivals in the passband of interest; *i.e.*, that the  
288 variability in LFE features (illustrated by the ‘Irregularity’ time series in Fig. 2a) will  
289 average to zero and for reasons described below, artifacts arising from the model’s  
290 periodicity lie outside this passband. The results of the simulations described in Section  
291 4, in which  $\tau_s$  varies, validate this proposal and are consistent with the predictions of this  
292 mathematical model. To illustrate the mathematical model more clearly we show the case  
293 in which the LFE signals do not overlap and  $\tau_s > \tau_c$  (top, Fig. 2a), and also the case more  
294 representative of overlapping LFE signals that manifest as tremor in which  $\tau_s < \tau_c$  (bottom,  
295 Fig 2a).



296

297 **Figure 2.** Theoretical model of clustered LFEs. (a) Cartoon of a model of a series of  
 298 identical pulses (pink) of width,  $\tau_c$ , arriving at regular intervals,  $\tau_s$ , and multiplied by an  
 299 envelope (gray shading, black curve) of width  $\tau_e$ . The top and bottom panels show the  
 300 cases in which  $\tau_s > \tau_c$  and  $\tau_s < \tau_c$ , respectively. (b) Specific example of the model in (a), in  
 301 which the envelope is a boxcar and the pulses have shapes and spectra similar to those of  
 302 LFEs. (c) Spectra of an LFE source (blue,  $P(f)$ ), a series of  $N$  delta functions (black,  
 303  $E(f)$ ), and the windowed series of LFEs (red,  $E(f)P(f)$ ). The spectrum of the windowed  
 304 LFE series is calculated analytically, for expressions (3), (5) and (6) and parameters  
 305 noted on the figure. Note that the amplitude of the flat portion of the spectrum is  $N$  times

306 that of a single LFE, the lowest corner frequency and spectral decay below this are  
 307 determined by the envelope shape and duration. See text for more explanation.  
 308

309 Our model includes two functions:  $p(t)$ , which describes the individual pulse shape (LFE  
 310 signal), and  $e(t)$ , which describes the shape of the envelope. In time both functions are  
 311 non-zero over limited ranges:  $p(t) \neq 0$  only if  $|t| \leq \tau_c/2$  and  $e(t) \neq 0$  only if  $|t| \leq \tau_e/2$ . (We use  
 312  $\tau_c$  to represent the pulse duration because its Fourier transform will contain a corner  
 313 frequency  $f_c$ ). The transient train of pulses in Figure 2a may be described by the  
 314 expression

$$315 \quad x(t) = e(t) \sum_{n=-\infty}^{n=\infty} p(t - n\tau_s) \quad (1)$$

316 where  $\tau_s$  is the spacing between pulses. This sum of LFE signals may be written more  
 317 compactly as

$$319 \quad x(t) = e(t) [c(t) * p(t)] \quad (2)$$

320 where  $c(t)$  is an infinite train of delta functions (often called a comb function) spaced at  
 321 intervals  $\tau_s$ , and the asterisk indicates convolution. In this model many LFE signals  
 322 arrive in the time span of the envelope function, so  $\tau_s \ll \tau_e$ . We denote the spectrum, or  
 323 Fourier transform of  $x(t)$  by  $X(f)$ , and use the convolution and similarity theorems of  
 324 Fourier theory, to express  $X(f)$  as

$$325 \quad X(f) = \tau_c \tau_s \tau_e P_{f_c}(f) [C_{f_s}(f) * E_{f_e}(f)] = \tau_c \tau_s \tau_e P_{f_c}(f) \sum_{n=-\infty}^{n=\infty} E_{f_e}(f - n f_s) \quad (3)$$

326 in which  $P(f)$ ,  $C(f)$  and  $E(f)$  are the Fourier transforms of  $p(t)$ ,  $c(t)$  and  $e(t)$ , and  $f_e = 1/\tau_e$ ,  
 327  $f_s = 1/\tau_s$ ,  $f_c = 1/\tau_c$ .

329  
 330 Expression (3) implies the Fourier transform of the pulse, or LFE, train is a series of  
 331 spectral peaks, each with the form  $E_{f_e}(f)$ , that repeat at frequency intervals  $f_s$ . The series of  
 332 peaks is windowed by the Fourier transform of the LFE,  $P_{f_c}(f)$ . As noted above, because  
 333 the series contains multiple pulses and  $f_e \ll f_s$ , the peaks are separated in frequency by  
 334 more than their bandwidth. The regular spacing of the peaks comes from the assumed  
 335 uniformity in the spacing of the LFE arrivals, and thus to some degree may be considered

336 an artifact of the model. Moreover, if numerous LFEs arrive within the cluster, or  $\tau_s$  is  
 337 sufficiently small, the frequency peaks at  $f_s=1/\tau_s$  and its multiples may be outside the  
 338 LFE and even the tremor passbands and thus can be neglected, since they would be  
 339 filtered out by the filtering needed to eliminate microseism and other noise; in most VLF  
 340 studies band-pass filters are used to retain energy between 0.01 and 0.05 Hz, while in  
 341 tremor and LFE studies only the 1-10 Hz energy is retained.

342

343 To this point we have not specified the shape of either the LFE signals or the envelope of  
 344 the cluster,  $p(t)$  or  $e(t)$ , respectively. Regardless of the precise shape of either, the  
 345 formulation above shows that the spectrum of a sum of clustered LFE signals is the  
 346 product of  $P(f)$  and  $E(f)$  (eqn. 3). Because the time-domain duration and frequency-  
 347 domain passband always vary inversely, the greater duration of  $e(t)$  means it will  
 348 determine the combined signal's characteristics at the lowest frequencies, and likely those  
 349 in the VLF pass band. In other words, the spectral characteristics are determined by the  
 350 envelope; the envelope may reflect the chance arrival pattern of multiple LFE signals,  
 351 some more coherent underlying source process, or some combination of these. This will  
 352 be true for any shape LFE or cluster envelope, because of the properties of "pulse-like"  
 353 functions with a finite area. We show in the Appendix that the Fourier spectrum of any  
 354 such pulse will have these properties: 1) approach a constant value at small frequencies,  
 355 and 2) decay at high frequencies at a rate  $f^{-n}$ , such that the function first becomes  
 356 discontinuous at the  $n$ -th time-derivative. The spectrum thus has zero- and high-  
 357 frequency asymptotes that always intersect at a corner frequency approximately equal to  
 358 the inverse of the pulse width.

359

360 In summary, the properties listed in the previous paragraph, and the fact that the envelope  
 361 is wider than an individual LFE, or  $f_e \ll f_c$ , imply that the spectrum will be described by a  
 362 flat portion for  $0 < f < f_e$ , a decay rate that depends on the envelope shape for  $f_e < f < f_c$ , and  
 363 for  $f > f_c$  a decay rate that is further modified by the shape of the LFE. In other words, at  
 364 frequencies below the LFE corner-frequency the spectrum is determined entirely by the  
 365 envelope, the shape of which is determined by interference pattern of multiple LFE  
 366 arrivals. The mathematical model in this Section shows all this to be true analytically.

367 While this requires the assumption of regular intervals between LFE signals, the resulting  
 368 artifacts lie outside the passband of interest. Moreover, the simulations presented in  
 369 Section 4 verify that these properties apply even when the intervals are highly variable.

370

371 We illustrate this theoretical model for a boxcar envelope, chosen because it is simple  
 372 and yields an analytic form for  $X(f)$ . Following [Hotovec et al., 2013] (Appendix A), the  
 373 Fourier transform of a Comb function is the series

$$374 \quad C\left(\frac{f}{f_s}\right) = \sum_{n=-\infty}^{\infty} \exp(-i2\pi n \frac{f}{f_s}) \quad (4)$$

375 The convolution of this with a boxcar that spans  $N$  LFE signals is equivalent to truncating  
 376 the series after  $N$  terms (Fig. 2b). This finite sum has the analytic form

$$377 \quad C\left(\frac{f}{f_s}\right) * E\left(\frac{f}{f_e}\right) = e^{(-i2\pi \frac{f}{f_s})} N \frac{\text{sinc}(\pi \frac{f}{f_e})}{\text{sinc}(\pi \frac{f}{f_s})} \quad (5)$$

378 In Figure 2c we show an example of a spectrum  $X(f)$  calculated according to expression  
 379 (5) and a Brune source model [Brune, 1970; 1971], or

$$380 \quad P\left(\frac{f}{f_c}\right) = M_0 \frac{1}{[1 + (\frac{f}{f_c})^2]} \quad (6)$$

381 We use parameters appropriate to those in real observations; i.e., a cluster duration  $\tau_e=20$   
 382 seconds,  $N=200$ ,  $\tau_s=\tau_e/N=0.1$  seconds, and  $\tau_c=0.5$  seconds or  $f_c=2$  Hz [Bostock et al.,  
 383 2015]. Note that when  $\tau_s < \tau_c$ , corresponding to LFE signals that overlap significantly, as  
 384 they would during bursts of tremor, the harmonics would occur above the VLF and  
 385 tremor passbands (red curve, Fig. 2c). Moreover, the harmonics arise because of the  
 386 periodicity assumed in order to derive an analytic model and thus may be considered to  
 387 be artifacts. As noted above, the simulations with variable  $\tau_s$  described in Section 4  
 388 demonstrate this, and that the precise spacing of the LFE signal arrivals is unimportant as  
 389 long as  $\tau_s < \tau_c$ . As predicted, the spectrum has a shape that largely reflects that of the  
 390 envelope of the clustered LFEs, with a lower corner frequency approximately equal to the  
 391 inverse of the envelope duration and a higher corner equal to that of the component LFE.  
 392 While a boxcar is an overly simplified representation of real envelopes, which will vary  
 393 from one LFE or tremor cluster to the next, we suggest it is a reasonable, first-order



394 representation. Interestingly, the spectrum decays as  $f^{-1}$  between about .02 and 2.0 Hz, as  
395 observed in several studies of VLF, LFE and tremor seismic signals.

396

397 In conclusion, regardless of the specific shape of the LFE or tremor source spectra, or of  
398 the envelope of a burst of arriving signals, the low-frequency attributes of the composite  
399 spectrum will reflect the characteristics of the latter. If one applies a narrow band-pass  
400 filter to remove all energy outside this low-frequency passband (as is often done to  
401 eliminate noise), there is then no way to tell the difference between a sequence of brief  
402 pulses (LFEs, tremor) spread over a longer time, and a single pulse (VLF source) acting  
403 over the same time. The corner frequency observed might thus be associated, not with the  
404 time during which a larger source slips, but with the time over which a sequence of  
405 smaller, similar events occurs in a kind of mini-swarm or simply arrive nearly  
406 simultaneously by chance. Additionally, the spectral decay rate of such a band-passed  
407 signal also may reflect only the manner in which a burst of multiple signals arrives in a  
408 short window, rather than the slip speed of a single slow source.

409

#### 410 **4. Synthetic VLF events**

411

412 In this section, we construct synthetic, idealized LFE signal clusters to test the idea that  
413 VLF events are just clusters of independent LFEs, rather than slow earthquakes resulting  
414 from a coherent slip event that is several orders of magnitude larger. Use of synthetics  
415 rather than real LFE signals has the benefit of avoiding the low-frequency noise that often  
416 obscures signals with periods of tens of seconds or more [Agnew and Berger, 1978;  
417 Berger et al., 2004; Barbour and Agnew, 2012]. We attempted to simulate VLF events  
418 using those of real LFEs, but found that the low frequency noise masked the signal in the  
419 VLF passband. To be sure that the low frequency energy in the summed signal was  
420 noise, we computed ratios of individual LFE waveforms in a single family and the  
421 family's 'template' LFE, and then stacked these ratios. The family's template should be  
422 nearly noise-free [William Frank, personal communication 2015] so that the ratio should  
423 remove the effect of coherent signals with any deviation from one representing  
424 incoherent noise. The noise at frequencies above the microseism peak did appear to

425 cancel when the ratios were stacked, evident as ratios equal to one, but did not at lower  
426 frequencies. We suspect that this is because destructive interference of noise by stacking  
427 requires noise to be stationary (its mean amplitude and standard deviation are invariant),  
428 which likely is not the case; although we did not test this rigorously, we suspect that  
429 occasionally the low frequency noise becomes extremely large and dominates the stack.

430

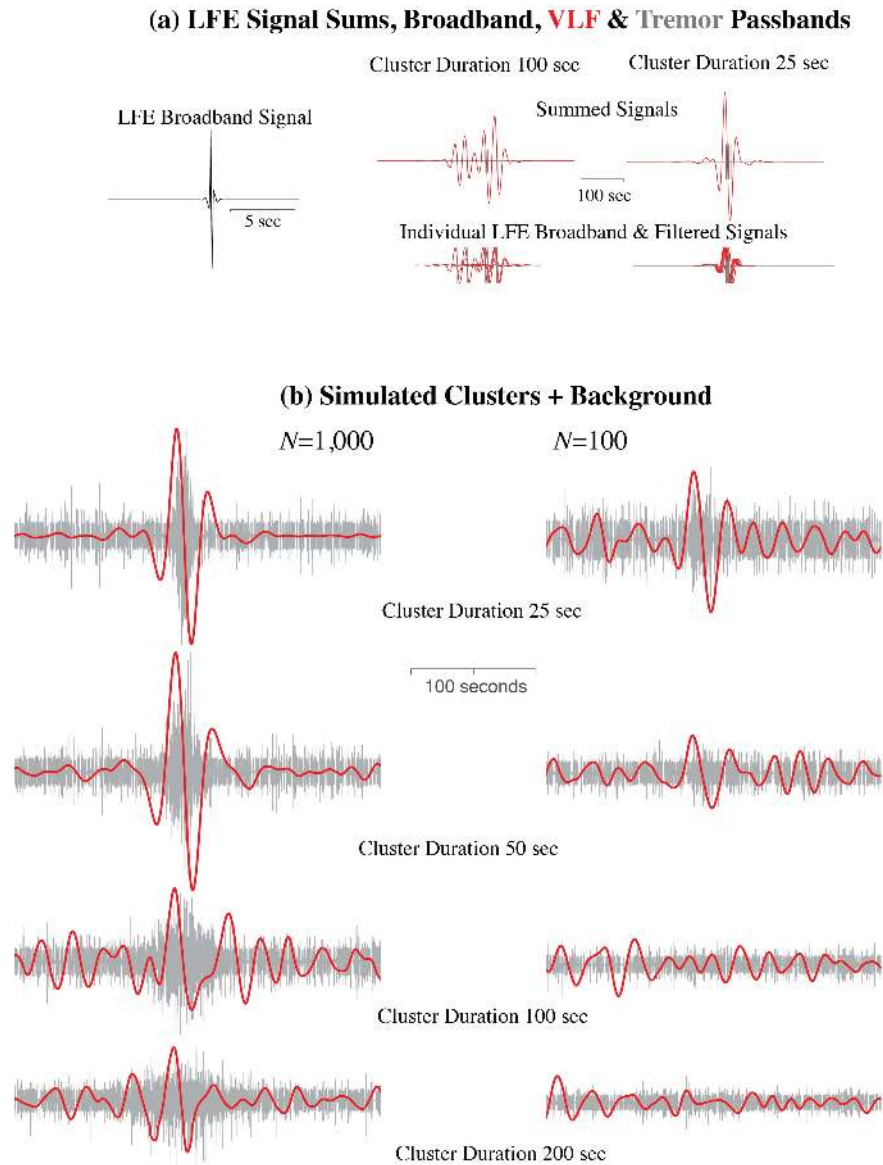
431 We simulate a velocity seismogram of an LFE by differentiating a delta function and  
432 low-pass filtering it with a corner frequency at  $f_c=3$  Hz and a high-frequency spectral  
433 decay rate of  $f^2$ . A zero-phase, 1<sup>st</sup>-order Butterworth filter accomplishes this. We choose  
434 3 Hz to be consistent with measured values for LFEs in Cascadia ( $f_c\sim 2-3$  Hz [Bostock *et al.*,  
435 2015]) and Parkfield, California ( $f_c\sim 5$  Hz [Thomas *et al.*, 2016]). Such a spectrum is  
436 consistent with an ‘omega-squared’ or ‘Brune’ earthquake source model [Brune, 1970;  
437 1971] and may appropriately represent the source spectrum of LFEs [Zhang *et al.*, 2011].  
438 As illustrated schematically in Figure 3a using only six (for clarity) of these synthetic  
439 LFE signals, when these signals arrive within an interval comparable or less than the  
440 dominant period of the pass-band of interest for VLF events ( $\sim 20-50$  sec period or  $\sim .02-$   
441  $.05$  Hz) and are filtered in this passband, the filtered waveforms add constructively when  
442 summed and a low frequency pulse results (right example, Fig. 3a). A zero-phase filter  
443 produces a pulse centered on the peak of the cluster (we use a 2<sup>nd</sup>-order Butterworth  
444 filter). Comparison of the with summed signals spread over a longer duration shows that  
445 such constructive interference and pulse-like waveforms diminish or disappear as filtered  
446 arrivals overlap by lesser amounts or not at all (left example, Fig. 3a). We test this more  
447 rigorously by generating a cluster of LFE signals, or equivalently a tremor burst, by  
448 summing  $N$  identical synthetic LFE signals that are time shifted with normally distributed  
449 random arrival times. We spread the arrivals of  $N$  LFEs over an interval that corresponds  
450 to an approximate tremor burst with duration,  $D$ , which is approximately equal to an  
451 interval of  $-3\sigma$  to  $+3\sigma$  in which  $\sigma$  is the standard deviation of the distribution of arrival  
452 times (*i.e.*, 99.7% of the  $N$  LFE signals arrive within the interval  $D$ ).

453

454 Figure 3b shows the results of band-pass filtering simulated clusters of  $N=100$  and  
455  $N=1,000$  LFE signals for different cluster durations, chosen to be similar to those in [Ide

456 *et al.*, 2008] (see their Figs. 3 and 4). To make these more realistic we have also added a  
457 ‘background’ of 2000 LFE signals that arrive at uniform randomly distributed times over  
458 an interval of 655 seconds. The results confirm the expectations described above and  
459 from the analytic model in Section 3 (but now without the regularity in LFE signal arrival  
460 times). Figure 3b shows that when the cluster duration is comparable to the period range  
461 of the passband, even a cluster of 100 LFEs produces a pulse-like signal when filtered in  
462 that passband and in the presence of background activity that is only slightly smaller than  
463 the cluster (i.e. the background rate of LFE signal arrivals is  $\sim 3/\text{sec}$  while that for the  
464 cluster is  $\sim 4/\text{sec}$ ). As the cluster duration spreads and/or it contains fewer arrivals, the  
465 apparent VLF event diminishes.

466



467

468 **Figure 3.** Simulated LFE cluster, in tremor and VLF pass-bands. **(a)** Schematic showing  
 469 how the duration of a cluster of LFE signals affects the coherent summing of low-  
 470 frequency components. Six copies of a simulated broadband velocity waveform (pulse  
 471 on left) that has been band-pass filtered in the tremor (2-8 Hz, grey) and VLF (.02-.05  
 472 Hz, red) passbands are distributed with random offsets. When filtered pulses are spread  
 473 over 50 sec (lower right) and they sum to form a pulse (upper right). When spread over  
 474 200 sec (lower center) the pulse-like character of the sum diminishes (upper center). **(b)**  
 475 Sum of  $N=100$  (right) and  $N=1000$  (left) of the filtered LFE signals in (a) with arrival  
 476 times sampled randomly from a normal distribution spread over the durations labeled and  
 477 added to a background of 655 sec containing LFES signals at 2000 uniformly-distributed  
 478 random times.

479

480

481 The characteristics of the VLF pulse that emerge from band-pass filtering a clustered sum

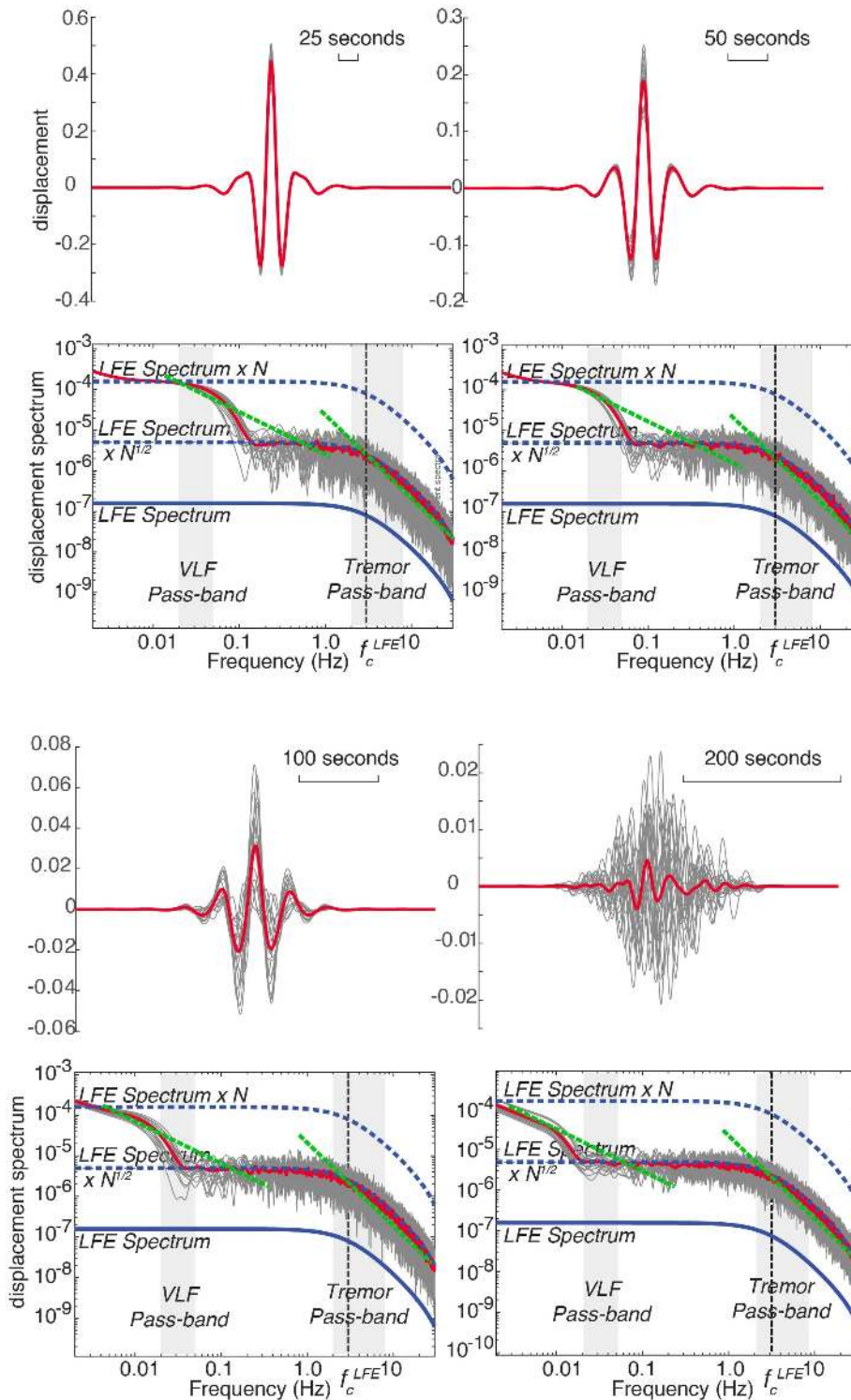
482 of LFEs, or a tremor burst, plausibly explain all the features of observed VLF events.  
 483 These features include 1) estimated magnitudes that are several orders of magnitude  
 484 larger than those of LFEs [Ide et al., 2008], 2) depletion in high frequencies relative to an  
 485 earthquake with comparable low frequency spectral amplitude [Ito et al., 2009; Takeo et  
 486 al., 2010], 3) spectral decay rates of  $\sim f^{-1}$  [Ide et al., 2007a], 4) waveforms that may be fit  
 487 with moment tensors consistent with the tectonic loading [Ito and Obara, 2006b; Ide et  
 488 al., 2008; Ito et al., 2009], and 5) source locations shared with those of tremor and LFE  
 489 sources [Ito and Obara, 2006a; Takeo et al., 2010; Walter et al., 2013]. We demonstrate  
 490 the consistency of these features with VLF waveforms that arise from summed LFE  
 491 signals in the examples that follow.

492

#### 493 4.1 Synthetic VLF and LFE magnitudes

494 The characteristics of the VLF events derived from a cluster of  $N$  LFE signals constructed  
 495 as described above are predictable. We first demonstrate how they explain the first VLF  
 496 feature noted above, that estimated VLF amplitudes are several orders of magnitude  
 497 larger than those of LFEs [Ide et al., 2008]. Each panel of Figure 4 shows the results for  
 498 20 individual simulations and their average, for cluster durations that vary by 20% around  
 499 the same durations as in Figure 3 (25, 50, 100, and 200 sec) but without the background  
 500 LFEs. The more clustered the LFEs are (the shorter the specified duration), the more  
 501 coherently the low-frequency spectral components add so that the summed VLF pulse  
 502 amplitude grows (note the different waveform amplitude scales in Fig. 4) and the low-  
 503 frequency spectral amplitude approaches a value that is  $N$  times greater than that of the  
 504 LFE (Fig. 4, bottom row). However, the higher frequency components sum incoherently  
 505 and if truly random, the summed spectral amplitudes will be  $N^{1/2}$  times as large as those  
 506 of an individual LFE signal. In summary, the spectrum of  $N$  summed clustered LFE  
 507 signals will have a low frequency spectral level approximately equal to that of a VLF  
 508 with  $M_0^{VLF} = N M_0^{LFE}$ , and high frequency spectral level equal to  $N^{1/2} M_0^{LFE}$  beyond the  
 509 corner frequency of the LFE (Fig. 4a, bottom row). We note that the increase by a factor  
 510 of  $N$  at low frequencies agrees with the analytic model presented in Section 3.

511



512

513 **Figure 4.** Effect of LFE cluster duration and variability on VLF waveforms. For each  
 514 duration, we show 20 realizations of simulated displacement waveforms (top) and spectra  
 515 (bottom) and their averages in grey and red, respectively. Absolute amplitude units are  
 516 arbitrary but the same for all simulations. In each realization  $N=1000$  identical LFE  
 517 signals (Fig. 3a) were summed and the sum band-pass filtered between .02-.05 Hz (see



518 text). Spectra of the LFE alone and multiplied by  $N$  and  $N^{1/2}$  are shown in solid and  
 519 dashed blue lines, respectively, and green dashed lines indicate spectral decay rates of  $f^1$   
 520 and  $f^2$ . Cluster durations are labeled and shown with scale bars.

521

522 We estimate the number of LFEs that must be summed to generate a VLF that is  $\Delta M_w$   
 523 moment magnitude units greater than the LFE's magnitude, and how the areas of  $N$  LFEs  
 524 might compare with that of a driving slow slip event, or SSE (top of Fig. 1b). From the  
 525 definition of moment magnitude,  $N=10^{\alpha M}$  with  $\alpha=1.5\Delta M$ . for example, the cases in  
 526 Figures 3 and 4 with  $N=1000$  LFE signals give rise to estimated VLF magnitudes 2.0  
 527 units larger than that of the LFE. If LFEs represent small, strong spots within  
 528 surrounding slowly slipping regions, then we need to ask if  $N$  LFEs may fit within such  
 529 regions. The ratio of the areas of  $N$  LFEs to that of a driving slow slip event may be  
 530 estimated assuming the source areas of both may be calculated as

$$531 \quad A=(M_0/k\Delta\tau)^{2/3} \quad (7)$$

532 in which  $M_0$  is seismic moment,  $k$  is a constant  $\sim 1$ , and  $\Delta\tau$  is stress drop [Aki, 1972].  
 533 Thus, the ratio of the areas of  $N$  non-overlapping LFEs to that of an SSE is  $N(M_0^{LFE}/M_0^{SSE})^{2/3}$   
 534  $(\Delta\tau^{SSE}/\Delta\tau^{LFE})^{2/3}$ . This ratio of LFE to SSE area plausibly could be less than one,  
 535 noting that the moments associated with the cumulative tremor or LFEs associated with  
 536 an accompanying SSE typically are orders of magnitude smaller [Kao et al., 2010; Ochi  
 537 and Kato, 2013]. Additionally, if LFE source areas overlapped, this effectively reduces  
 538  $N$ . Finally, while estimation of stress drops of LFEs are highly uncertain because the slip  
 539 and areas can only be inferred very indirectly [Sweet et al., 2014; Bostock et al., 2015],  
 540 the ratio of SSE to LFE stress drops most likely is  $\leq 1$ ; e.g., Sweet et al. [2014] estimate  
 541  $\Delta\tau^{LFE}$  could be between a few kPa to several MPa. Typically, when measured  
 542 geodetically  $\Delta\tau^{SSE}$  estimates are more well constrained, with values in the range of  $\sim 10$ -  
 543 100 kPa [Gao et al., 2012].

544

#### 545 *4.2 Synthetic VLF and LFE high frequency depletion*

546 The second VLF feature to explain is the VLF depletion in high frequencies relative to an  
 547 earthquake with comparable low frequency spectral amplitude [Ito et al., 2009; Takeo et  
 548 al., 2010]. As noted above and illustrated in Figure 4, the apparent moment of the VLF  
 549 event, or cluster of LFEs, is  $M_0^{VLF}=NM_0^{LFE}$  and the corner frequency,  $f_c$ , of LFE cluster is

550 the same as that for a single LFE signal,  $f_c^{LFE}$ . We relate  $f_c$  to  $M_0$  using the definitions for  
 551 stress drop (eqn. 7) and corner frequency,  $f_c$ ,

$$552 \quad f_c = (2.34V/2\pi)(k\Delta\tau/M_0)^{1/3} \quad (8)$$

553 with  $V$  denoting rupture velocity. To guarantee that the apparent VLF is depleted in high  
 554 frequencies relative to an earthquake with the same moment, or  $M_0^{eq} = NM_0^{LFE}$ , requires  
 555 that  $f_c^{eq} > f_c^{LFE}$ , with superscript *eq* referring to earthquake values. Assuming similar  
 556 rupture velocities for the LFE and earthquake (both must be close to the shear velocity to  
 557 be seismic), this requirement implies

$$558 \quad (\Delta\tau^{eq}/M_0^{eq})^{1/3} > (\Delta\tau^{LFE}/M_0^{LFE})^{1/3} \quad \text{or} \quad \Delta\tau^{eq} > N\Delta\tau^{LFE} \quad (9)$$

559 *Bostock et al.* [2015], *Sweet et al.* [2014] and [*Thomas et al.*, 2016] have estimated  $\Delta\tau$  for  
 560 LFE signals, and *Shelly et al.* [2007] showed stacks of spectra for LFEs, earthquakes, and  
 561 tremor (their Fig. 2). Results of these studies indicate LFE corner frequencies, and  
 562 inferred  $\Delta\tau$  values, are less than those for earthquakes of comparable magnitudes by  
 563 several orders of magnitude. Estimates of  $\Delta\tau$  by *Brodsky and Mori* [2007] for large  
 564 ‘tsunami’ (slow rupturing) earthquakes do not differ significantly from faster  
 565 earthquakes, but those for relatively aseismic creep events lasting days or longer are  
 566 lower by an order of magnitude or more. *Fletcher and McGarr* [2011] estimated that  $\Delta\tau$   
 567 for tremor events were more than an order of magnitude smaller than those of  
 568 earthquakes, and in their analysis of VLF P-waves *Ito and Obara* [2006b] concluded that  
 569 their  $\Delta\tau$  values were 2-3 orders of magnitude smaller than the range for earthquakes of  
 570 comparable moment. These studies and our synthetic examples suggest the requirement  
 571 of equation (9) may be satisfied.

572

### 573 *4.3 Synthetic VLF and LFE spectral decay rate*

574 The third feature to explain is the spectral decay rate of  $\sim f^{-1}$ . Figure 4 shows the spectra  
 575 of summed LFEs, for four different cluster durations. At frequencies above the VLF  
 576 pass-band the spectral components add randomly and the spectrum is simply a scaled  
 577 version of the LFE spectrum, by a factor of  $N^{1/2}$ . At lower frequencies the spectrum of  
 578 the cluster envelope dominates, and approaches a level  $N$  times that of an individual LFE



579 signal. These  $N^{1/2}$ - and  $N$ -fold increases are expected for signals that add randomly and  
 580 coherently, respectively, noting that as the cluster duration decreases the low frequency  
 581 spectral components add more constructively and the spectrum becomes flatter. The  
 582 addition of noise and some variability in the component LFEs would likely smooth these  
 583 idealized spectra, yielding spectra that may decay as  $f^{-1}$  from the lowest measurable  
 584 frequency to approximately  $f_c^{LFE}$ . Even if not describable precisely as  $f^{-1}$ , these examples  
 585 show that the decay rate will be slower than the  $f^{-2}$  that typifies earthquakes. Although  
 586 not shown, if the LFE spectral decay rate is close to  $f^{-1}$  instead of  $f^{-2}$  as assumed in the  
 587 example, the summed LFE signal would decay as  $f^1$  or slower for the entire spectrum.  
 588

#### 589 *4.4 Synthetic VLF and LFE moment tensors*

590 Finally, we consider the similarity between moment tensors and hypocenters estimated  
 591 from VLF, LFE and tremor signals (4<sup>th</sup> and 5<sup>th</sup> features). Synthetic tests show that the  
 592 shape of the VLF pulse is a longer period version of the LFE waveform, and does not  
 593 change significantly when the cluster duration varies by  $\pm 20\%$ . Thus, if the LFEs and  
 594 tremor (assumed to be comprised of LFEs) are consistent with tectonically sensible  
 595 moment tensors or hypocenters, the band-passed signal derived from a cluster of  
 596 randomly-summed LFEs also will be. Hypocenter estimates are constrained primarily by  
 597 the move-out patterns of the arrival times of VLF centroids, so that as long as the  
 598 clustering of the component LFEs does not vary significantly across the network, the  
 599 move-out pattern and hypocenter estimates also should be very similar to that of the  
 600 centroid of the LFE distribution.

601

### 602 **5. Observational Evidence from Costa Rica**

603

604 Support for VLF events representing a single, coherent slip event would be given by  
 605 observations of them when smaller slip events were not occurring; *i.e.*, in the absence of  
 606 active tremor or LFE. Although a failure to find VLF events without concurrent tremor  
 607 or LFE clusters does not rule out the possibility of a single, larger coherent slip event, it  
 608 does support our proposal that interpretation of VLF events is non-unique. Here we  
 609 describe observations from the northern Costa Rica subduction zone during several 5-14

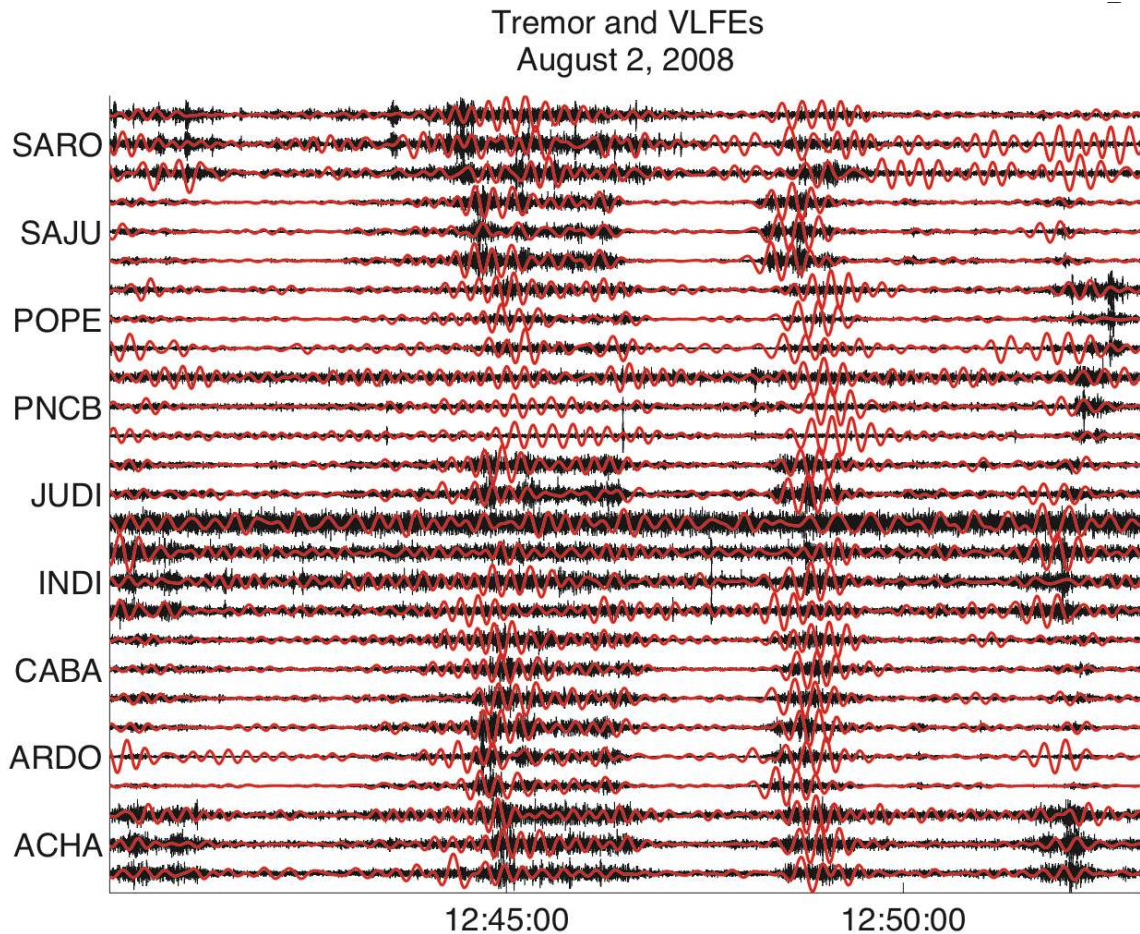
610 day shallow slow slip events that show VLF events only occurring during tremor  
611 episodes and never as isolated events. Tests comparing spectral amplitudes of tremor and  
612 VLF events to those predicted by our analytic model and simulations would be useful,  
613 but are beyond the scope of this study.

614

615 The seismogenic zone beneath the Nicoya Peninsula, Costa Rica exhibits diverse slip  
616 behavior including normal earthquakes, slow slip, tremor, low and very low frequency  
617 earthquakes. During the last 163 years, four large megathrust earthquakes occurred  
618 beneath the Nicoya Peninsula: 1853, 1900, 1950 (Mw 7.7) and 2012 (Mw 7.6) [*Protti,*  
619 2014]. Since 2003 GPS and seismic networks on the Nicoya Peninsula have recorded ten  
620 slow slip events accompanied by tremor [*Outerbridge et al., 2010; Walter et al., 2011;*  
621 *Jiang et al., 2012; Dixon et al., 2014*]. Large slow slip events repeat every  $21 \pm 6$  months,  
622 with smaller events occurring much more frequently [*Jiang et al., 2012; Dixon et al.,*  
623 2014]. All of the SSEs are accompanied by tremor with both LFE and VLF events  
624 detected within this tremor [*Brown et al., 2009; Walter et al., 2013*]. Tremor is routinely  
625 located using envelope cross-correlation methods and in general, is poorly located.

626

627 *Walter et al. [2013]* documented the synchronous occurrence of geodetically detected  
628 slow slip, tremor and VLF events at shallow depth offshore the Nicoya Peninsula in  
629 August 2008. During the first week of August 2008, they identified 54 VLF events.  
630 Figure 5 shows 15 minutes of seismic data during this time period illustrating the VLF  
631 events embedded within the tremor. The temporal overlap between the tremor bursts and  
632 VLF events is a ubiquitous characteristic.

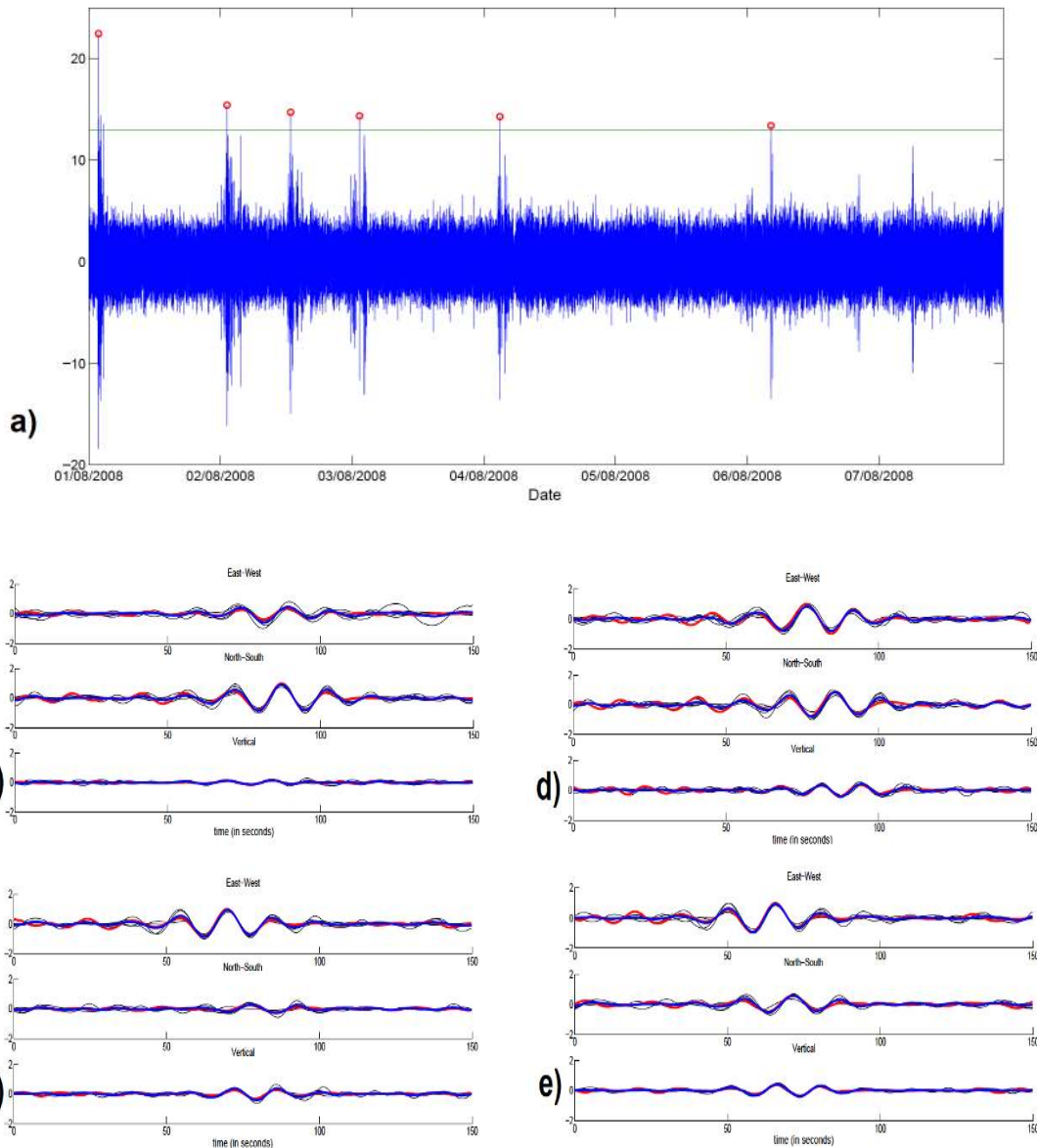


633  
634  
635  
636  
637  
638

**Figure 5.** Example of amplitude normalized very low frequency events (12-30s band-pass filtered) embedded within higher frequency (2-8 Hz band-pass filtered) tremor during the August 2008 northern Costa Rica slow slip event.

639 We used the events in the *Walter et al.* [2013] VLF catalog as candidate template events  
640 and applied a matched filter technique to identify additional VLF events during this and  
641 three other slow slip episodes. VLF events with high signal-to-noise ratios at 5 or more 3-  
642 component stations were retained as template events. The periods of time investigated  
643 had both geodetically determined slow slip and abundant tremor and included: May 16-  
644 22, 2007, July 31- August 7, 2008, March 1-10 and June 20-27, 2009, and October 8-26,  
645 2010. For all intervals, continuous velocity time series were filtered between 12-30 s and  
646 down sampled to 1 Hz. The technique computes the cross-correlation values between the  
647 template event and continuous data at each sample point to obtain a cross-correlation  
648 function (CCF). The CCFs for all stations and components are then stacked to produce a

649 single summed CCF. Detection occurs when the summed CCF exceeds a threshold value  
 650 similar to other studies utilizing a network-based matched-filter [Shelly *et al.*, 2007]. An  
 651 example of the summed CCF, positive event detections and VLF waveforms for a 2008  
 652 template and its matches is shown in Figure 6.



653

654

655

656 **Figure 6.** a) Result of the cross-correlation (blue trace) between a template VLF in 2008  
 657 and 7 days of data (filtered in the passband 12-30s). The highest peak corresponds to the  
 658 cross-correlation of the template with itself. The smaller peaks above the threshold (green  
 659 line) correspond to matches. b)-e) Waveform comparisons for stations ACHA, ARDO,  
 660 CABA, and SAJU respectively, between the template (red trace), the 5 matches (black  
 661 traces) and the stack of all the matches in this time interval (blue trace). For each event,  
 662 all trace amplitudes are normalized to the peak value at that station.



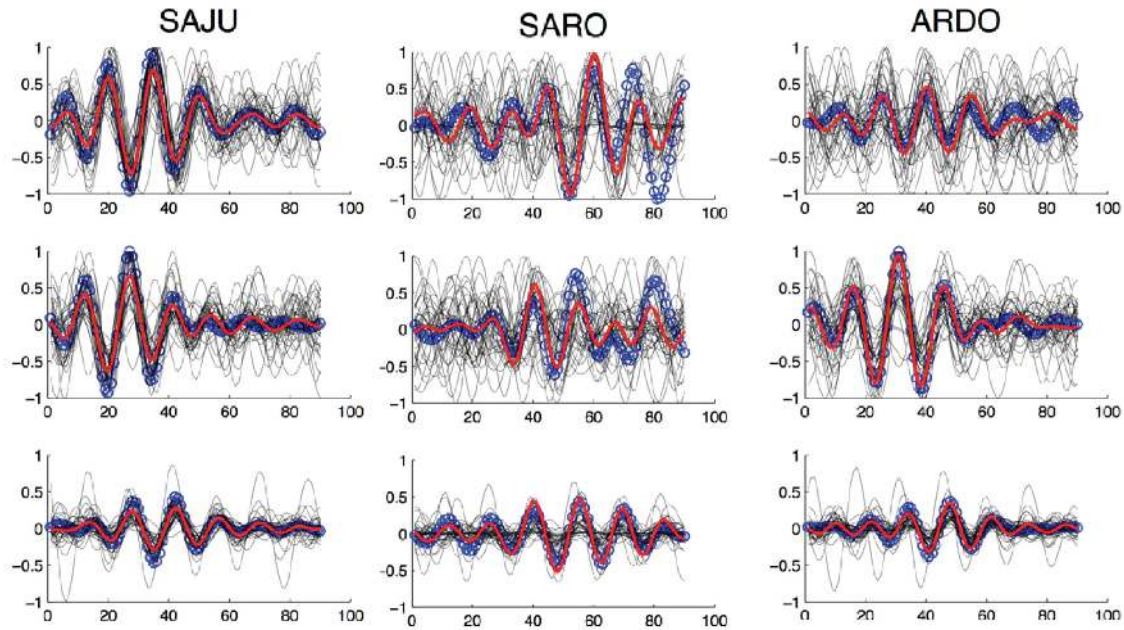
663

664 We identified VLF events that repeated over multiple SSE episodes by cross-correlating  
665 the templates identified in 2008, and their highest quality matches, and selecting all time  
666 periods with summed CCFs that exceeded our threshold. In total we have detected over  
667 one hundred VLF events using five different template events. An example of a high  
668 quality template event and the matches it identifies through the entire time period  
669 (excerpts of 2007-2010) is shown in Figure 7. Each template identifies positive  
670 detections during all slow slip events that show remarkable waveform similarity, leading  
671 us to conclude that discrete patches of the fault plane are consistently reactivated during  
672 subsequent SSE episodes. The dimensions of these patches cannot be resolved but are  
673 likely within several tens of km, which is the location uncertainty of some of the VLF  
674 sources. If VLF events are comprised of signals from multiple LFE sources, they may be  
675 separated by comparable distances. We also visually identified several VLF events that  
676 were distinct from the original templates and cross-correlated them through the time  
677 period of interest. These templates also yielded many matches, revealing the existence of  
678 distinct template families.

679

680 Application of this matched-filter search to all four years of continuous data is beyond the  
681 scope of this study; however our finding that all VLF detections are synchronous with  
682 tremor (2-8 Hz), which itself occurs less than 10% of the time (~90 hours of 1248 hours  
683 analyzed), supports the hypothesis that VLF events represent a superposition of LFE  
684 arrivals observed through a low pass filter. These VLF events, as well as the tremor they  
685 are embedded within, are located by cross-correlating envelopes in both the low and high  
686 frequency bands. VLF events detected with templates from different families yield  
687 distinct source locations (different by  $> 25$  km) while synchronous VLF and tremor,  
688 regardless of their template family, always produce indistinguishable locations  
689 considering their uncertainties of as much as 20 km.

690



691 **Figure 7.** Oct 9, 2010 template and matching velocity waveforms for three stations.  
 692 Similarity between the template event (red trace), the matches (black traces) and the  
 693 stack of all waveforms (blue trace) is excellent even though waveforms span the time  
 694 period between 2007-2010. All 3-component (top: east, middle: north, bottom: vertical)  
 695 data are normalized by station.  
 696

697  
 698  
 699  
 700

## 6. Discussion and Conclusions

701 Although VLF pulses produced by band-pass filtering a clustered sum of LFEs share  
 702 characteristics with observed VLF events this does not rule out the possibility that some  
 703 VLF events may originate from single, much larger coherent slow earthquakes.  
 704 However, the ubiquitous simultaneity of VLF with tremor and LFE signals, particularly  
 705 during tremor bursts, suggests that many VLF events could be clusters of independently  
 706 rupturing and radiating LFEs. We have used theoretical and synthetic models to show  
 707 that a cluster of LFE signals or tremor produces the characteristics of VLF events, and,  
 708 most importantly, that the key VLF attributes used to infer source characteristics may  
 709 instead arise from the envelope or shape of the cluster. While a VLF event may be  
 710 radiated from transient slow slip that propagates coherently and quasi-dynamically over  
 711 dimensions of tens of kilometers, it also may result from a superposition of signals from  
 712 slip on numerous smaller patches with dimensions of tens of meters that rupture at higher  
 713 velocities. These latter LFEs may be triggered by a single aseismic slow slip front

714 propagating coherently over tens of km, or by spatially and mechanically distinct but  
715 nearly simultaneous smaller aseismic slip events. Additionally, as in regular earthquakes  
716 and aftershocks, clusters of LFEs may arise because they interact with one another (e.g.  
717 via dynamic or static stress transfer) or possibly even by chance superposition of multiple  
718 background LFEs that fail due to constant tectonic loading. In the interpretation of a  
719 VLF event as a single, dynamic slip event we would expect that VLF events would  
720 occasionally be observed without accompanying higher-frequency tremor or LFE signals.  
721 While not proving the alternative interpretations, analyses of continuous data from Costa  
722 Rica recorded over periods of 8 to 20 days each in the years 2007 through 2010, yielded  
723 no detections of VLF events in the absence of tremor. Although tremor occurred during  
724 less than 10% of these periods, matched-filter template scanning through all these data  
725 detected VLF events only concurrent with the tremor.

726

727 We suggest that the VLF observations may be interpreted in terms of three end-member  
728 source models. These each have different implications for the scaling of slip events with  
729 size and slip mode, from fast earthquakes to slow effectively-aseismic transient slip. We  
730 discuss scaling in the context of inferred  $M_0$  versus event duration,  $T$ , proposed initially in  
731 *Schwartz and Rokosky* [2007] and *Ide et al.* [2007b; 2008].

732

733 The first interpretation considers VLF events to originate from  $M_w$ 2-5 slow seismic  
734 sources that scale with  $M_0$  proportional to  $T$  [*Schwartz and Rokosky*, 2007; *Ide et al.*,  
735 2007b; 2008] (steeper grey band in Fig. 8). In their interpretation  $M_0$  versus  $T$  scaling  
736 differs for ‘slow’ and ‘fast’ slip events, reflecting fundamentally different source  
737 processes. We note that even these authors acknowledge inconsistencies between slow  
738 scaling and VLF measurements. For example, *Ide et al.* [2008] measured  $M_0$  proportional  
739 to  $T^{3/2}$ , but dismissed this deviation from the conventional scaling as an “artifact of the  
740 limited frequency range of our analysis, 0.005–0.05 Hz”. Later *Ide* [2008] suggested  $M_0$   
741 is proportional to  $T^2$  and proposed a different physical model than that in *Ide et al.*  
742 [2007b]. We also note that the same inference offered by *Zhang et al.* [2011] to explain  
743 tremor spectra, may also apply to VLF measurements, that they scale like regular  
744 earthquakes but have lower stress drops and/or slower, but still seismic, rupture

745 propagation velocities (e.g., dotted lines in Fig. 8).

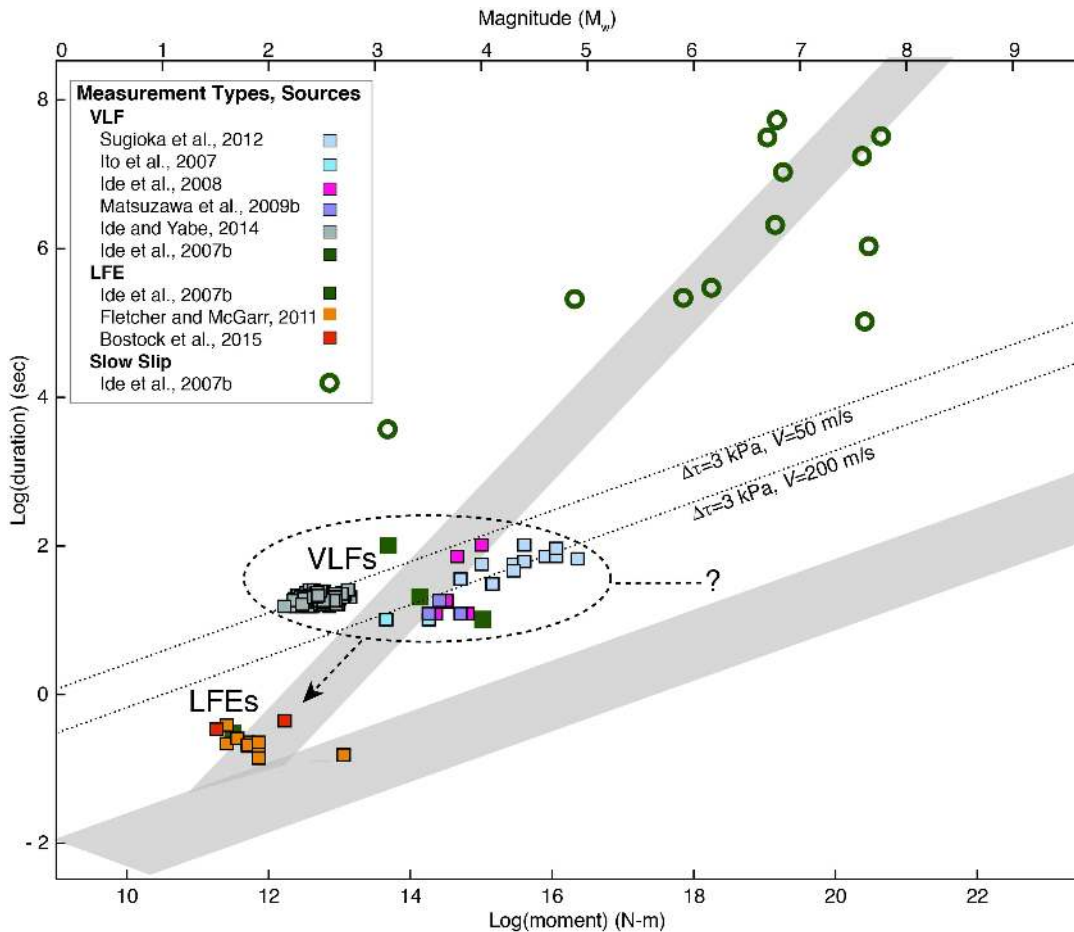
746

747 The model proposed by *Ide* [2008] appears to fit in this first class, and highlights the non-  
748 uniqueness in interpreting the VLF and LFE observations. In this model, VLF events  
749 represent radiation from transient coherent slip from slip events for which the  $M_0$  versus  
750  $T$  scaling differs from earthquakes. For each event, the slipping region is assumed to  
751 grow overall, but with "random expansion and contraction" according to an  
752 autoregressive model; the resulting fluctuations in moment rate give rise to tremor. *Ide*  
753 [2008] noted that the noise-free version of this model does not predict the occurrence of  
754 LFE signals as observed, instead predicting durations orders of magnitude longer. *Ide*  
755 [2008] suggests that LFE scaling results from only observing radiated energy above the  
756 noise threshold, which has a briefer duration. So in this model VLF events would be  
757 directly caused by the slip, with the LFE signals being a second-order byproduct: nearly  
758 the opposite of our interpretation.

759

760 The second and third interpretations consider VLF events to result from the clustered  
761 arrival of LFE or tremor signals, but clustered for two different reasons. In the second  
762 interpretation, the LFE sources result from passage of a slow, effectively aseismic, slip  
763 front passing across a fault containing the tiny seismogenic asperities that fail and  
764 efficiently radiate seismic waves, much like swarms and aftershocks driven by  
765 spontaneous slow slip and afterslip, or as in the laboratory as acoustic emissions that  
766 accompany slow preslip [*McLaskey and Lockner, 2014*]. Thus, in this interpretation VLF  
767 events serve as proxies indicative of causative, much larger, slower moment release, and  
768 provide only a lower bound on its magnitude (Fig. 8, dashed horizontal line and question  
769 mark). However, as in aftershock sequences, *Frank et al.* [2016] note that in some  
770 regions clustering of LFEs does not simply reflect the speed-up of LFE failure rates as  
771 slow slip fronts pass, but the latter actually enhances mechanisms by which LFE patches  
772 interact with one another (e.g. via static or dynamic stress transfer). Thus, while  
773 associated with larger scale slow slip, other processes may be important in controlling  
774 LFE clustering.





775

776 **Figure 8.** Slip event scalar moment,  $M_0$ , versus duration,  $T$ , observations and scaling  
 777 relationships. Inferred slow and fast (steeper and shallower grey bands, respectively)  
 778 scaling relations are shown with seismic and geodetic measurements (solid and open dark  
 779 green squares and circles, respectively) of slow slip events reported in [Ide *et al.*, 2007b].  
 780 Published VLF and LFE measurements are shown as squares, with colors assigned to the  
 781 study each are reported in (see legend). Dotted lines through the VLF events correspond  
 782 to fast slip scaling calculated for stress drop and rupture velocities estimated for VLF  
 783 events [Matsuzawa *et al.*, 2009b].

784

785 The third, end member interpretation is that the clustering of LFEs need not result  
 786 directly from a spatially or temporally coherent process like a driving, slower slip  
 787 transient, but rather may be more like the clustering that appears in more standard  
 788 earthquake seismicity as part of the variability inherent in a Poisson process [Michael,  
 789 2012] . Results shown in Frank *et al.* [2016] may corroborate this as they note that  
 790 clustered LFEs occur both during and between times of slow slip events in southern  
 791 Mexico. While they showed that time series of the recurrence intervals of many  
 792 individual LFEs are non-Poissonian, their observations do show that temporally and

793 spatially clustered LFEs occur in the absence of geodetically detectable slow slip. In this  
 794 case the VLF moment-duration observations serve only as proxies for LFEs (diagonal  
 795 dashed arrow in Fig. 8). Given all these alternatives, we conclude that VLF events do  
 796 not provide discriminants between  $M_0$  versus  $T$  scaling models.

797

## 798 **Appendix A**

799 We show here that the Fourier spectrum of a time-limited, finite area pulse will have  
 800 these properties: 1) approach a constant value at small frequencies, 2) decay at high  
 801 frequencies at a rate  $f^{-n}$ , such that the function first becomes discontinuous at the  $n$ -th  
 802 time derivative, and 3) have zero- and high-frequency asymptotes that always intersect at  
 803 a corner frequency approximately equal to the inverse of the pulse width. The first  
 804 property arises from the definition of the Fourier integral, which at zero frequency is just  
 805 the integral over the function, and so is nonzero if the function has a finite area. To first  
 806 order this area will be  $A \tau$ , where  $A$  is the amplitude and  $\tau$  the time constant, and if  
 807 we take  $X(f)$  to be this up to a corner frequency  $f_c$ , then  $f_c = \tau$ . The second fact arises  
 808 by noting that when the  $(n-1)$ th derivative of  $x(t)$  has a discontinuity, the  $n$ th derivative of  
 809 the discontinuity is a delta function, so that if there are  $D$  discontinuities at  $t_d, d=1,..D$ .

$$810 \quad \begin{aligned} \frac{d^n x(t)}{dt^n} &= \sum_{d=1}^D \delta(t-t_d) & t = t_d \\ &= \frac{d^n x(t)}{dt^n} & t \neq t_d \end{aligned} \quad (\text{A.1})$$

811 Since the Fourier transforms of a time derivative of a function equals the product of the  
 812 function's spectrum and  $2\pi if$ , and that of a delta function equals one,  $X(f)$  may be written

$$813 \quad X(f) = (2\pi if)^{-n} \frac{d^n X(f)}{dt^n} = (2\pi if)^{-n} \left[ \sum_{d=1}^D e^{-2\pi if t_d} + \frac{d^n X(f)}{dt^n} \right] \quad (\text{A.2})$$

814 The contribution of the discontinuities is constant and thus dominates over that of the  
 815 derivatives at high frequencies, so that to first order,

$$816 \quad |X(f)| \approx (2\pi if)^{-n} \left[ 1 + 2 \frac{d^n X(f)}{dt^n} \right] \approx (2\pi if)^{-n} \quad (\text{A.3})$$

817

818

819 **References**

820

821 Agnew, D. C., and J. Berger (1978), Vertical seismic noise at very low frequencies, *J.*  
 822 *Geophys. Res.*, *83*(B11), 5420–5424, doi:10.1029/JB083iB11p05420.

823 Aki, K. (1972), Earthquake Mechanism, *Tectonophysics*, *13*, 423–446.

824 Aki, K., and P. G. Richards (1980), *Quantitative Seismology, Theory and Methods*, New  
 825 York.

826 Ando, R., N. Takeda, and T. Yamashita (2012), Propagation dynamics of seismic and  
 827 aseismic slip governed by fault heterogeneity and Newtonian rheology, *J. Geophys.*  
 828 *Res.*, *117*(B11), B11308–14, doi:10.1029/2012JB009532.

829 Armbruster, J. G., W.-Y. Kim, and A. M. Rubin (2014), Accurate tremor locations from  
 830 coherent S and P waves, *J. Geophys. Res.*, *119*, 1–14, doi:10.1002/(ISSN)2169-9356.

831 Asano, Y., K. Obara, and Y. Ito (2008), Spatiotemporal distribution of very-low  
 832 frequency earthquakes in Tokachi-oki near the junction of the Kuril and Japan  
 833 trenches revealed by using array signal processing, *Earth Planets Space*, *60*, 871–  
 834 875.

835 Barbour, A. J., and D. C. Agnew (2012), Detection of seismic signals using seismometers  
 836 and strainmeters, *Bulletin of the Seismological Society of America*, *102*(6), 2484–  
 837 2490, doi:10.1785/0120110298.

838 Berger, J., P. Davis, and G. Ekström (2004), Ambient Earth noise: A survey of the Global  
 839 Seismographic Network, *J. Geophys. Res.*, *109*(B11), 1–10,  
 840 doi:10.1029/2004JB003408.

841 Bostock, M. G., A. A. Royer, E. H. Hearn, and S. M. Peacock (2012), Low frequency  
 842 earthquakes below southern Vancouver Island, *Geochem. Geophys. Geosyst.*, *13*(11),  
 843 1–12, doi:10.1029/2012GC004391.

844 Bostock, M. G., Thomas, A. M. Thomas, G. Savard, L. Chuang, and A. M. Rubin (2015),  
 845 Magnitudes and moment-duration scaling of low-frequency earthquakes beneath  
 846 southern Vancouver Island, *J. Geophys. Res.*, *120*, 1–22, doi:10.1002/(ISSN)2169-  
 847 9356.

848 Brodsky, E. E., and J. Mori (2007), Creep events slip less than ordinary earthquakes,  
 849 *Geophys. Res. Lett.*, *34*(16), n/a–n/a, doi:10.1029/2007GL030917.

850 Brown, J. R., G. C. Beroza, S. Ide, K. Ohta, D. R. Shelly, S. Y. Schwartz, W. Rabbel, M.  
 851 Thorwart, and H. Kao (2009), Deep low-frequency earthquakes in tremor localize to  
 852 the plate interface in multiple subduction zones, *Geophys. Res. Lett.*, *36*, L19306–5,  
 853 doi:10.1029/2009GL040027.

- 854 Brune, J. N. (1971), Correction to Tectonic stress and the spectra, of seismic shear waves  
855 from earthquakes, *J. Geophys. Res.*, 76, 5002.
- 856 Brune, J. N. (1970), Tectonic stress and the spectra of seismic shear waves from  
857 earthquakes, *J. Geophys. Res.*, 75(26), 4997–5009, doi:10.1029/JB075i026p04997.
- 858 Chamberlain, C. J., D. R. Shelly, J. Townend, and T. A. Stern (2014), Low-frequency  
859 earthquakes reveal punctuated slow slip on the deep extent of the Alpine Fault, New  
860 Zealand, *Geochem. Geophys. Geosyst.*, 15(7), 2984–2999,  
861 doi:10.1002/2014GC005436.
- 862 Dixon, T. H., Y. Jiang, R. Malservisi, R. McCaffrey, N. Voss, M. Protti, and V. Gonzalez  
863 (2014), Earthquake and tsunami forecasts: Relation of slow slip events to subsequent  
864 earthquake rupture, *Proc Natl Acad Sci USA*, 111(48), 17039–17044,  
865 doi:10.1073/pnas.1412299111.
- 866 Fletcher, J. B., and A. McGarr (2011), Moments, magnitudes, and radiated energies of  
867 non-volcanic tremor near Cholame, CA, from ground motion spectra at UPSAR,  
868 *Geophys. Res. Lett.*, 38(16), 1–7, doi:10.1029/2011GL048636.
- 869 Frank, W. B., N. M. Shapiro, A. L. Husker, V. Kostoglodov, A. A. Gusev, and M.  
870 Campillo (2016), The evolving interaction of low-frequency earthquakes during  
871 transient slip, *Science Advances*, 2(4), e1501616–e1501616,  
872 doi:10.1126/sciadv.1501616.
- 873 Frank, W. B., N. M. Shapiro, V. Kostoglodov, A. L. Husker, M. Campillo, J. S. Payero,  
874 and G. A. Prieto (2013), Low-frequency earthquakes in the Mexican Sweet Spot,  
875 *Geophys. Res. Lett.*, 40(11), 2661–2666, doi:10.1002/grl.50561.
- 876 Frank, W. B., N. Shapiro, A. Husker, V. Kostoglodov, A. Romanenko, and M. Campillo  
877 (2014), Using systematically characterized low frequency earthquakes as a fault  
878 probe in Guerrero, Mexico, *J. Geophys. Res.*, 1–15, doi:10.1002/(ISSN)2169-9356.
- 879 Frankel, A. (1995), Simulating strong motions of large earthquakes using recordings of  
880 small earthquakes: the Loma Prieta mainshock as a test case, *Bulletin of the*  
881 *Seismological Society of America*, 85, 1144–1160.
- 882 Gao, H., D. A. Schmidt, and R. J. Weldon (2012), Scaling relationships of source  
883 parameters for slow slip events, *Bulletin of the Seismological Society of America*,  
884 102(1), 352–360, doi:10.1785/0120110096.
- 885 Gardonio, B., D. Marsan, O. Lengliné, B. Enescu, M. Bouchon, and J.-L. Got (2015),  
886 Changes in seismicity and stress loading on subduction faults in the Kanto region,  
887 Japan, 2011–2014, *J. Geophys. Res.*, 120, 2616–2626, doi:10.1002/(ISSN)2169-  
888 9356.
- 889 Ghosh, A., E. Huesca-Pérez, E. E. Brodsky, and Y. Ito (2015), Very low frequency  
890 earthquakes in Cascadia migrate with tremor, *Geophys. Res. Lett.*, 1–5,

- 891 doi:10.1002/(ISSN)1944-8007.
- 892 Gomberg, J., K. Creager, J. Sweet, J. Vidale, A. Ghosh, and A. Hotovec (2012),  
 893 Earthquake spectra and near-source attenuation in the Cascadia subduction zone, *J.*  
 894 *Geophys. Res.*, *117*(B5), B05312–12, doi:10.1029/2011JB009055.
- 895 Hartzell, S., S. Harmsen, A. Frankel, and S. Larsen (1999), Calculation of Broadband  
 896 Time Histories of Ground Motion: Comparison of Methods and Validation using  
 897 Strong-Ground Motion from the 1994 Northridge Earthquake, *Bulletin of the*  
 898 *Seismological Society of America*, *89*, 1484–1504.
- 899 Hotovec, A. J., S. G. Prejean, J. E. Vidale, and J. Gomberg (2013), Strongly gliding  
 900 harmonic tremor during the 2009 eruption of Redoubt Volcano, *Journal of*  
 901 *Volcanology and Geothermal Research*, *259*(C), 89–99,  
 902 doi:10.1016/j.jvolgeores.2012.01.001.
- 903 Hutchison, A. A., and A. Ghosh (2016), Very low frequency earthquakes  
 904 spatiotemporally asynchronous with strong tremor during the 2014 episodic tremor  
 905 and slip event in Cascadia, *Geophys. Res. Lett.*, *43*(13), 6876–6882,  
 906 doi:10.1002/2016GL069750.
- 907 Ide, S. (2008), A Brownian walk model for slow earthquakes, *Geophys. Res. Lett.*,  
 908 *35*(17), L17301–5, doi:10.1029/2008GL034821.
- 909 Ide, S. (2014), Modeling fast and slow earthquakes at various scales, *Proc. Jpn. Acad.*,  
 910 *Ser. B*, *90*(8), 259–277, doi:10.2183/pjab.90.259.
- 911 Ide, S. (2016), Characteristics of slow earthquakes in the very low frequency band:  
 912 Application to the Cascadia subduction zone, *J. Geophys. Res.*, *121*, 1–33,  
 913 doi:10.1002/2016JB013085.
- 914 Ide, S., and S. Yabe (2014), Universality of slow earthquakes in the very low frequency  
 915 band, *Geophys. Res. Lett.*, 1–19, doi:10.1002/(ISSN)1944-8007.
- 916 Ide, S., D. R. Shelly, and G. C. Beroza (2007a), Mechanism of deep low frequency  
 917 earthquakes: Further evidence that deep non-volcanic tremor is generated by shear  
 918 slip on the plate interface, *Geophys. Res. Lett.*, *34*(3), L03308–5,  
 919 doi:10.1029/2006GL028890.
- 920 Ide, S., G. C. Beroza, D. R. Shelly, and T. Uchide (2007b), A scaling law for slow  
 921 earthquakes, *Nature*, *447*(7140), 76–79, doi:10.1038/nature05780.
- 922 Ide, S., K. Imanishi, Y. Yoshida, G. C. Beroza, and D. R. Shelly (2008), Bridging the gap  
 923 between seismically and geodetically detected slow earthquakes, *Geophys. Res. Lett.*,  
 924 *35*(10), L10305–6, doi:10.1029/2008GL034014.
- 925 Ito, Y., and K. Obara (2006a), Dynamic deformation of the accretionary prism excites  
 926 very low frequency earthquakes, *Geophys. Res. Lett.*, *33*(2), L02311–4,

- 927 doi:10.1029/2005GL025270.
- 928 Ito, Y., and K. Obara (2006b), Very low frequency earthquakes within accretionary  
929 prisms are very low stress-drop earthquakes, *Geophys. Res. Lett.*, *33*(9), L09302–4,  
930 doi:10.1029/2006GL025883.
- 931 Ito, Y., K. Obara, K. Shiomi, S. Sekine, and H. Hirose (2007), Slow earthquakes  
932 coincident with episodic tremors and slow slip events, *Science*, *315*(5811), 503–506,  
933 doi:10.1126/science.1134454.
- 934 Ito, Y., K. Obara, T. Matsuzawa, and T. Maeda (2009), Very low frequency earthquakes  
935 related to small asperities on the plate boundary interface at the locked to aseismic  
936 transition, *J. Geophys. Res.*, *114*, B00A13–16, doi:10.1029/2008JB006036.
- 937 Jiang, Y., S. Wdowinski, T. H. Dixon, M. Hackl, M. Protti, and V. Gonzalez (2012),  
938 Slow slip events in Costa Rica detected by continuous GPS observations, 2002–2011,  
939 *Geochem. Geophys. Geosyst.*, *13*(4), 1–18, doi:10.1029/2012GC004058.
- 940 Kao, H., K. Wang, H. Dragert, J. Y. Kao, and G. Rogers (2010), Estimating seismic  
941 moment magnitude (  $M_w$ ) of tremor bursts in northern Cascadia: Implications for the  
942 “seismic efficiency” of episodic tremor and slip, *Geophys. Res. Lett.*, *37*(19), n/a–n/a,  
943 doi:10.1029/2010GL044927.
- 944 Lengliné, O., and J.-P. Ampuero (2015), Insights on earthquake triggering processes from  
945 early aftershocks of repeating microearthquakes, *J. Geophys. Res.*, *120*, 6977–6992,  
946 doi:10.1002/(ISSN)2169-9356.
- 947 Matsuzawa, T., K. Obara, and T. Maeda (2009a), Source duration of deep very low  
948 frequency earthquakes in western Shikoku, Japan, *J. Geophys. Res.*, *114*, B00A11–  
949 10, doi:10.1029/2008JB006044.
- 950 Matsuzawa, T., K. Obara, and T. Maeda (2009b), Source duration of deep very low  
951 frequency earthquakes in western Shikoku, Japan, *J. Geophys. Res.*, *114*, B00A11–  
952 10, doi:10.1029/2008JB006044.
- 953 McLaskey, G. C., and D. Lockner (2014), Preslip and cascade processes initiating  
954 laboratory stick slip, *J. Geophys. Res.*, *119*, 1–14, doi:10.1002/(ISSN)2169-9356.
- 955 Michael, A. J. (2012), Fundamental questions of earthquake statistics, source behavior,  
956 and the estimation of earthquake probabilities from possible foreshocks, *Bulletin of*  
957 *the Seismological Society of America*, *102*(6), 2547–2562, doi:10.1785/0120090184.
- 958 Nadeau, R. M., and T. V. McEvilly (1999), Fault Slip Rates at Depth from Recurrence  
959 Intervals of Repeating Microearthquakes, *Science*, *285*, 718–721.
- 960 Ochi, T., and T. Kato (2013), Depth extent of the long-term slow slip event in the Tokai  
961 district, central Japan: A new insight, *J. Geophys. Res.*, *118*(9), 4847–4860,  
962 doi:10.1002/jgrb.50355.

- 963 Outerbridge, K. C., T. H. Dixon, S. Y. Schwartz, J. I. Walter, M. Protti, V. Gonzalez, J.  
964 Biggs, M. Thorwart, and W. Rabbel (2010), A tremor and slip event on the Cocos-  
965 Caribbean subduction zone as measured by a global positioning system (GPS) and  
966 seismic network on the Nicoya Peninsula, Costa Rica, *J. Geophys. Res.*, *115*(B10),  
967 B10408–17, doi:10.1029/2009JB006845.
- 968 Peng, Z., and J. Gomberg (2010), An integrated perspective of the continuum between  
969 earthquakes and slow-slip phenomena, *Nature*, *3*(9), 599–607, doi:10.1038/ngeo940.
- 970 Protti, M. (2014), Nicoya earthquake rupture anticipated by geodetic measurement of the  
971 locked plate interface, *Nature Geosci.*, *7*(12), 117–121, doi:10.1038/ngeo2038.
- 972 Royer, A. A., and M. G. Bostock (2014), A comparative study of low frequency  
973 earthquake templates in northern Cascadia, *Earth and Planetary Science Letters*,  
974 *402*(C), 247–256, doi:10.1016/j.epsl.2013.08.040.
- 975 Rubin, A. M., and J. G. Armbruster (2013), Imaging slow slip fronts in Cascadia with  
976 high precision cross-station tremor locations, *Geochem. Geophys. Geosyst.*, *14*(12),  
977 5371–5392, doi:10.1002/ggge.20305.
- 978 Rubinstein, J. L., D. R. Shelly, and W. L. Ellsworth (2010), Non-volcanic Tremor: A  
979 Window into the Roots of Fault Zones, pp. 287–314, Springer Netherlands,  
980 Dordrecht.
- 981 Savard, G., and M. G. Bostock (2015), Detection and location of low-frequency  
982 earthquakes using cross-station correlation, *Bulletin of the Seismological Society of*  
983 *America*, *105*(4), 2128–2142, doi:10.1785/0120140301.
- 984 Schwartz, S. Y., and J. M. Rokosky (2007), Slow slip events and seismic tremor at  
985 circum-Pacific subduction zones, *Rev. Geophys.*, *45*(3), 1–32,  
986 doi:10.1029/2006RG000208.
- 987 Shelly, D. R., G. C. Beroza, and S. Ide (2007), Non-volcanic tremor and low-frequency  
988 earthquake swarms, *Nature*, *446*(7133), 305–307, doi:10.1038/nature05666.
- 989 Shelly, D. R., G. C. Beroza, S. Ide, and S. Nakamura (2006), Low-frequency earthquakes  
990 in Shikoku, Japan, and their relationship to episodic tremor and slip, *Nature*,  
991 *442*(7099), 188–191, doi:10.1038/nature04931.
- 992 Sweet, J. R., K. C. Creager, and H. Houston (2014), A family of repeating low-frequency  
993 earthquakes at the downdip edge of tremor and slip, *Geochem. Geophys. Geosyst.*,  
994 *15*(9), 3713–3721, doi:10.1002/2014GC005449.
- 995 Takeo, A. et al. (2010), Very broadband analysis of a swarm of very low frequency  
996 earthquakes and tremors beneath Kii Peninsula, SW Japan, *Geophys. Res. Lett.*,  
997 *37*(6), 1–5, doi:10.1029/2010GL042586.
- 998 Thomas, A. M., G. C. Beroza, and D. R. Shelly (2016), Constraints on the source

- 999 parameters of low-frequency earthquakes on the San Andreas Fault., 1–8,  
1000 doi:10.1002/(ISSN)1944-8007.
- 1001 Walter, J. I., S. Y. Schwartz, J. M. Protti, and V. Gonzalez (2011), Persistent tremor  
1002 within the northern Costa Rica seismogenic zone, *Geophys. Res. Lett.*, *38*(1), 1–5,  
1003 doi:10.1029/2010GL045586.
- 1004 Walter, J. I., S. Y. Schwartz, M. Protti, and V. Gonzalez (2013), The synchronous  
1005 occurrence of shallow tremor and very low frequency earthquakes offshore of the  
1006 Nicoya Peninsula, Costa Rica, *Geophys. Res. Lett.*, *40*(8), 1517–1522,  
1007 doi:10.1002/grl.50213.
- 1008 Wech, A. G., and K. C. Creager (2011), A continuum of stress, strength and slip in the  
1009 Cascadia subduction zone, *Nature Geosci.*, *4*(9), 624–628, doi:10.1038/ngeo1215.
- 1010 Yamashita, Y. et al. (2015), Migrating tremor off southern Kyushu as evidence for slow  
1011 slip of a shallow subduction interface, *Science*, *348*(6235), 676–679.
- 1012 Zhang, J., P. Gerstoft, P. M. Shearer, H. Yao, J. E. Vidale, H. Houston, and A. Ghosh  
1013 (2011), Cascadia tremor spectra: Low corner frequencies and earthquake-like high-  
1014 frequency falloff, *Geochem. Geophys. Geosyst.*, *12*(10), n/a–n/a,  
1015 doi:10.1029/2011GC003759.

1016

1017 **Acknowledgements**

1018 The authors thank Amanda Thomas, David Shelly, Honn Kao and two anonymous  
1019 reviewers for their helpful reviews and comments. Seismic data from Costa Rica can be  
1020 obtained through the IRIS DMC (Nicoya Network code YZ).